AN EXPERIMENTAL INVESTIGATION OF THE DYNAMIC FRACTURE OF A BRITTLE MATERIAL

Thesis by

Gordon Carl Smith

In Partial Fulfillment of the Requirements

For the Degree of

Doctor of Philosophy

California Institute of Technology

Pasadena, California

1975

(Submitted April 15, 1975)

ACKNOWLEDGEMENTS

I would like to express my gratitude to my advisor, Dr. Wolfgang Knauss, for his encouragement and suggestions during this investigation. I also extend my appreciation to Dr. Charles Babcock for many valuable discussions.

I am indebted to Mr. C. Hemphill for patient assistance in the laboratory, to Mrs. E. Fox for cheerfully typing this manuscript, and to Mrs. B. Wood for skillfully drawing the figures.

The support of this work by the California Institute of Technology is also gratefully acknowledged.

ABSTRACT

A new method of experimentally investigating the behavior of a crack in a stress wave environment has been developed and used to study the initial stages of dynamic crack propagation in Homalite 100, a polyester. The experimental method, which employs an electromagnetic loading device, permitted the application of pressure pulses to the surfaces of an 18 inch crack. The amplitude (51 psi to 1020 psi) and duration ($\sim$ 200 μsec) of the pulses were highly repeatable. The experimental configuration simulates, in the vicinity of the crack tip, a tension wave impacting a stationary semi-infinite crack in an infinite two-dimensional body where the wave front is parallel to the crack. A high speed framing camera, synchronized with the loading device, was used to record the time required for the crack to begin to propagate and its subsequent extension and velocity. The experimental results were analyzed within the bounds of linearly elastic fracture mechanics and a correlation was made between the dynamic stress intensity factor and the time at which the cracks began to propagate. It was found that the critical stress intensity factor increased dramatically with increasing loading rates at very high rates, which contrasts with quasi-static loading where the critical stress intensity factor decreases with an increasing loading rate. A simple model suggests that temperature effects at the crack tip may account for the observed increase in the critical stress intensity factor at high loading rates. Crack branching of running cracks was observed but unlike previous reports of branching, the cracks in this study branched mostly into three separate fast-running cracks.

TABLE OF CONTENTS

1. INTRODUCTION

The origin of fracture mechanics is generally accepted to have been established by Griffith [1] in 1921. Prior to that time, there did not exist a satisfactory explanation of why the observed strength of materials was so much lower than that predicted from theoretical consideration of the molecular binding forces. Griffith postulated that the observed reduction in strength was due to the stress concentrating effect of flaws and cracks that naturally occur in materials. This point of view is now generally accepted and it is interesting to note that one can now, some fifty years after Griffith's work, fabricate specimens in which flaws and cracks are held to a minimum, so that strengths on the order of theoretical predictions are observable [2].

Since Griffith's original postulation and experimental work with glass, numerous investigators have extended the original concept to include other types of materials such as those that exhibit locally at the crack tip plastic or viscoelastic behavior. These latter material phenomena significantly influence the stress and/or strain field near a crack tip and consequently the fracture process of the material. Such extensions of the simplified view of brittle fracture, in many cases, serve as excellent models for engineering design and analysis.

As the problems associated with static or near static loading conditions became more clearly understood and in some cases resolved, some investigators have begun to direct their attention to the more difficult problem of dynamic fracture. The latter are

generally defined to be those fracture events in which inertial effects are significant. The motivation in dynamic fracture stems from the numerous practical engineering situations associated with blast impact loading on structures. Often the question that is crucial in dynamic fracture is whether or not some critical value defining the onset of crack propagation is exceeded. This question arises in the design of aircraft or spacecraft subject to impact from objects such as meteorites, projectiles, or even birds or rain in the case of windshields or radomes. Other examples where the onset of dynamic fracture can be vitally important are machinery and power plants subject to impact damage, seismic disturbance, thermal shock, or cavitation in adjacent fluids.

The present work is intended to contribute to understanding the problem of initial crack growth under dynamic loading. The particular objectives of the work reported here pertain to the following:

a) does the static criterion for fracture hold at much higher rates of loading?

b) is a rate sensitivity criterion applicable at the high rates?

c) if fracture is rate dependent, what is the nature of that dependency?

To answer these questions, an electromagnetic stress wave generator was assembled and synchronized with a high speed camera to study the response of a single crack when a dynamic (pressure) load is applied to the crack faces.

This thesis is divided into seven chapters. The next chapter contains a review of related work previous to that reported here. It has theoretical and experimental sections and generally follows the chronological development of the field. The stress wave nature of the problem imposed some constraints and special considerations that are discussed in Chapter 3. The two chapters following that discussion contain a description of the equipment and the results of the equipment calibration respectively. Chapter 6 is a summary of the test data obtained from ten dynamic fracture experiments, while Chapter 7 is devoted to the analysis of the results as well as discussion of their implication.

2. PREVIOUS WORK

A. Theoretical

In a review [5] of the work on the dynamics of fracture, Erdogan in 1968 concludes that "compared to other areas of research dealing with the mechanical response of deformable solids the field (of dynamic fracture) is in a rather primitive stage." The theoretical work reported on the subject of dynamic fracture can be classified as comprised of either dimensional type analyses relying on either energy considerations, or analyses through solution of the dynamic equations of the linearized theory of elasticity. A review of the contributions to the field using energy methods is contained in Reference [6]. The principle employed in these works is a balance between work and energy where the energy is distributed as strain energy, kinetic energy and energy associated with new surfaces resulting from fracture. The energy method has typically yielded a relation for crack velocity as a function of rate independent material properties and crack length and has provided an estimate of the terminal velocity of the crack. In a series of recent papers Steverding and Lehnigk depart from previous approaches and in a simplified continuum analysis used the conservation of angular momentum principle along with an energy balance to find a minimum stress pulse duration and intensity to initiate crack propagation [7, 8, 9].

Until recently the solutions of the dynamic equations of elasticity have been limited to cases involving constant crack tip velocities. These solutions (the first of which appeared in 1951)

are discussed by Sih [11]. A particular problem in this class, namely that of a semi-infinite stationary crack that is impacted by a plane tension wave as shown in Figure 1 is pertinent to the

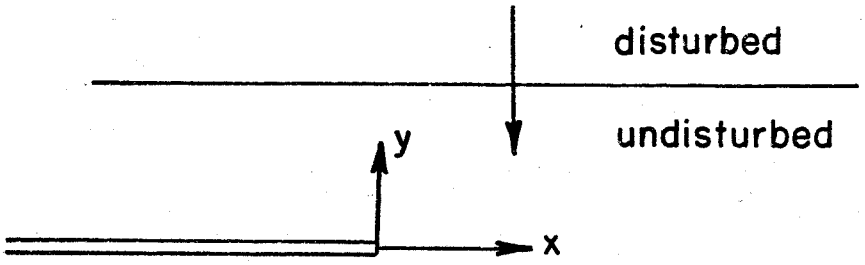

FIG. 1

present study. The problem has been solved by Maue [12], Ang [13], and as a special case by Baker [14]. A simplifying step taken in the solution of the problem was to decompose the problem into two parts that could be solved independently; namely, the suddenly pressurized crack and the planar stress wave in an uncracked medium. These are shown in Figure 2. A principal result of these solutions is of particular interest here; namely, the asymptotic form of the stress in the vicinity of the crack tip. The form given by Baker (discussed by Achenbach and Nuismer [15]) is shown below where T is the amplitude of the stress pulse, x is the distance from the crack tip, $F_+(0)$ is a constant arising from Baker's Wiener-Hopf factorization, C_s is the equivoluminal wave speed, and t denotes time.

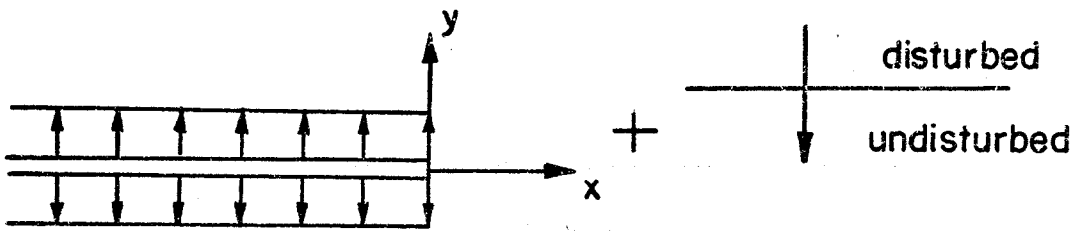

FIG. 2

$$\sigma_y(x, 0, t) \sim \frac{2T}{\pi F_+(0)} \left(\frac{t}{C_s x}\right)^{\frac{1}{2}} \quad \text{as } t/x \to \infty \qquad (1)$$

The stress given above becomes singular as the distance from the crack tip tends toward zero. The coefficient of the singularity is commonly referred to as the (dynamic) stress intensity factor K and is widely used in fracture work to characterize the elastic field in the vicinity of the crack tip.

Atkinson and Eshelby [16] and Freund [17] have shown for the case of dynamic fracture that the strain energy release rate, G, depends only on the elastic field in the neighborhood of the crack tip. This quantity plays a central role in the theory of fracture and is discussed further in the chapter on the analysis of the experimental data. Another result given by Freund [18] that was useful to this study is a Green's function that can be used to determine the stress intensity factor for a loading on the faces of a crack that is symmetric with respect to the crack axis but otherwise arbitrary in regard to space and time. There have been a number of other recent solutions giving dynamic stress intensity factors in a variety of geometric and loading conditions. These will be listed only as they

do not bear directly on the work reported here. Among these are solutions of the dynamic equation of elasticity by Achenbach [19], Sih, Embley and Ravera [20], Thau and Lu [21], Freund [22, 23, 24], and Freund and Rice [25].

B. Past Experimental Work

The experimental work in the field of dynamic fracture can be classified as being concerned with either spallation or running cracks. The spallation approach depends on naturally occurring material without artificially induced cracks and has a tradition dating back to work in 1872 by J. Hopkinson [26] who measured the strength of steel wires when they were suddenly stretched by a falling weight. The principal conclusion of these and subsequent similar tests by B. Hopkinson [27] was that the strength of steel wire was much greater under dynamic stress conditions than under static conditions. B. Hopkinson [28] also investigated the fractures produced in metal specimens when small quantities of explosives were detonated in contact with them. With thick plates (greater than $\frac{1}{2}$" in thickness) the surface of the plate that was in contact with the explosive was found to be dented and a circular disc of metal had been thrown off from the opposite face. Kolsky and Shearman [29] and Kolsky and Christie [30] performed similar experiments on smaller specimens of transparent materials. This type of specimen permitted observation of fractures produced by the interference between reflected pressure pulses. Recent investigations of dynamic fracture employing flat plates propelled by light gas guns have been reported by Curran, Shockey, and Seamen [31]. Spallation

investigations have provided extremely important information for the understanding of fracture. Typically spallation work is concerned with fracture events that originate at microcracks and that occur during fractions of a microsecond. This investigation was to be concerned with dynamic fracture under better defined stress states near individual crack tips and thus the experimental approach used in spallation studies did not seem to be the most advantageous.

The running crack work can be characterized by its emphasis on the dynamic behavior of one or more clearly identifiable cracks. The earliest work of this kind was reported by Schardin and Struth [32, 33] in 1937 and 1938. Using a multiple spark camera with a framing rate of about 300,000/sec, they attempted to record the response of a projectile being shot into a water box having glass windows. Schardin [34] writes "The glass windows of the box were destroyed and the surprising and interesting result was found that the front of the fractures was bound by a circle indicating that the velocity of fracture in this instance was constant." Crack velocity values were obtained as a function of material constituents, applied stress, temperature and composition of ambient atmosphere. The terminal velocity of the propagating cracks was found to be independent of the applied stress level, but it was affected by changes in the chemical composition of the glass. Similar results have been found subsequently by other investigators and a summary of the terminal velocities found is presented in Table 1 below.

Table 1

Maximum Crack Velocities

Investigator	Material	$C_{max} \cdot (E/\rho)^{-\frac{1}{2}}$
Schardin [35]	Glass	0.34-0.61
Cotterell [36]	PMMA	0.29-0.39
Dulaney and Brace [37]	PMMA	0.33-0.36
Roberts and Wells [38]	Steel	0.20-0.42
Wells and Post [39]	CR-39	0.38
Beebe [40]	Homalite	0.24
Bradley and Kobayashi [4]	Homalite	0.24

Following in the tradition of Schardin's pioneering work, and using the technique of ultrasonic fractography developed by Kerkhof [41], Küppers [42] was able to determine crack acceleration rates to an accuracy not achieved by high speed photography.

The dynamic fracture experiment involving a running crack is not suited for the study of the onset of dynamic fracture since the specimen is loaded statically* until the crack begins to run, thereby supplying the dynamic content to the experiment after the time span of interest in the present work. Some information concerning the onset problem, however, might be inferred from that type of experiment. In the work by Bradley and Kobayashi [4] the

---

*The inertia of the grips and hardware associated with mechanical test machines have thus far posed serious problems to those who have attempted to place a true dynamic tension boundary condition on the edge of a plate [40].

stress intensity factor at the arrest (abrupt stopping) of a fast running crack in Homalite was determined by photoelastic methods. The stress intensity factor at arrest was found to be 30 percent below that found under quasi-static conditions. From this result one might infer that a polymeric material such as Homalite is less fracture resistant at the rates of loading associated with dynamic events. The results discussed here later on support that inference.

3. DISCUSSION OF EXPERIMENTAL CONSTRAINTS

A. Loading Conditions

The approach used in theoretical treatments of decomposing fracture problems into the problem of a pressurized crack and an uncracked plate (see Figure 2, for example) suggests that an experimental analog is appropriate. This prospect is enhanced by the fact that the contribution to the singular stress near the crack tip (see Eqn. 1) is entirely due to the pressurized crack solution. For this approach to be feasible, it is necessary to employ a method whereby a pressure pulse could be applied on a timescale characterized by microseconds and in a quite confined location; i.e., along crack surfaces. A method that depended on electromagnetic forces was found to be highly suitable for this application. Snell, MacKallor and Guernsey [54] had successfully used this technique to apply a nearly sinusoidal pressure pulse to the edge of a plate and studied the behavior of stress waves as they propagated through a region containing a circular hole. A schematic of how the magnetic pressure was employed in the present crack growth initiation study is shown in Figure 3.

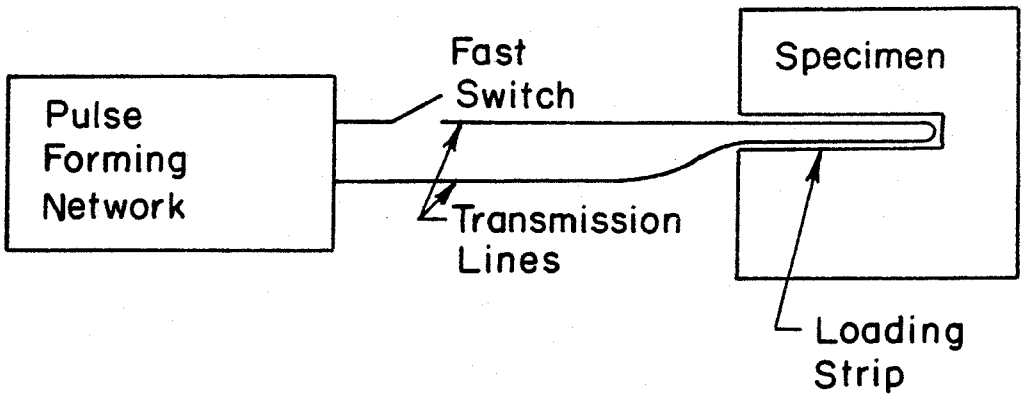

FIG. 3. Schematic of Fracture Experiment

It is easy to show (see Meagher [43] for example) that if two conducting strips are separated by a thin insulator (thin relative to the width of the strips, w) with a magnetic permeability μ, then the perpendicular force per unit area resulting from the current i flowing in opposite directions is given by

$$P = \tfrac{1}{2}\mu(i/w)^2 \qquad (2)$$

Since the pressure is proportional to the square of the current, it is possible to prescribe, within bounds, a pressure history by the choice of an appropriate current-forming network. Several of the theoretical treatments discussed in Chapter 2 assumed a step loading on the crack faces and it therefore seemed desirable to approximate that loading history in this experimental effort. If the resistance in a current-forming network is sufficiently small to preclude non-linear effects resulting from heating, the normalized current shape is independent of the amplitude of the current. It is therefore possible to prescribe a family of load histories that differ only in amplitude. Geometric dispersion considerations and data acquisition considerations were dominant factors in establishing the time frame of the current pulse and are discussed in subsequent sections.

B. Material Selection

The material selected for the experimental program was Homalite 100* which is a polyester and hereafter called Homalite.

---

*Supplied by the Homalite Corporation, Wilmington, Delaware.

Metals occur much more frequently in structures than do plastics and thus would seem to be more likely candidates for specimens in fracture experiments. However, for an initial effort, Homalite seemed to be an excellent experimental material. There is also considerable interest in the fracture behavior of polymeric materials. Homalite and other plastics have been widely used for dynamic fracture experiments. Some investigators use Homalite to simulate metals primarily because it is easy to machine and transparent so that (internal) fracture processes can be readily followed. Homalite is viscoelastic although at the rates of loading associated with stress waves and at room temperature, the relaxation modulus response is "glassy" and largely insensitive to loading rates [40]. This may not be true at the crack tip where the strains and strain gradients are high and this is one of the questions this study sought to answer. Homalite has several advantageous properties. On a macroscopic scale, it is essentially homogeneous and isotropic and exhibits birefringence which can be exploited as described later. In a previous fracture investigation [44], it was found that structural variables in annealed crystalline metals caused considerable complications. Homalite was used as the specimen material in the dynamic fracture experiments of Beebe [40], Bradley and Kobayashi [4], and Dalley, Fourney and Halloway [60], and its dynamic photoelastic properties have also been reported by Clark and Sanford [45].

C. Specimen Geometry

All of the theoretical work discussed previously had as a basic assumption the condition of plane strain. It was decided early in this work to make the experiments as compatible as possible with existing solutions. The two major obstacles to that objective were the locally three-dimensional character of the stress state near the crack tip and the possibility of geometric dispersion due to the finite dimensions of practical specimen geometries. The three-dimensional character of the crack tip is of course not limited to dynamic fracture problems but occurs in any type of fracture where the crack intersects a free surface. However, for a material such as Homalite that fails in a "brittle" manner (i.e., no observable necking at the crack tip), the plane strain description is reasonable. Away from the crack tip where the plate thickness is the characteristic length instead of the crack tip "radius," an approximation related to minimizing dispersive effects was found necessary and is discussed in the subsequent paragraphs.

There are two basic approaches that can be chosen to minimize the dispersive effects. The first of these would be to employ a sufficiently thick model in order to isolate the area of interest from free edges that could cause dispersion. Attempts to devise a specimen geometry according to that criterion led to unwieldy configurations that were not particularly compatible with the electromagnetic loading technique.

The other approach, which was selected, depended on the use of plates that were thin relative to the wavelengths of the Fourier components that form the stress wave. Boundary loading of a plate theoretically could generate an infinity of modes, but it has been shown by Miklowitz [46] and Miklowitz and Nisewanger [47] for the case of a rod that the lowest mode of wave propagation dominates at least for some initial time interval. One would expect the same situation for a plate. Figure 4 shows the wave velocity for the lowest mode of propagation in an infinite plate [48] where C_p is the plate velocity, d is the plate thickness, and Λ is the wavelength. Thus for a mildly dispersive wave, the plate thickness must be small compared to the wavelength associated with the highest significant frequency of a Fourier decomposition of the stress wave. Conversely, the choice of a plate thickness establishes a limit above which frequencies cannot be allowed if dispersion is to be mild. The result of restricting high frequency components of what would otherwise be a sharp step is essentially a "smoothed" step with a finite risetime.

For the purpose of selecting an appropriate risetime, a series of idealized wave forms based on what could be achieved with the electromagnetic loading device were constructed. Each sample wave corresponding to different risetimes was decomposed into frequency components. Scott and Miklowitz [49] give a relationship for phase velocity as a function of wavelength, which was used to compute the phase shifts after the wave had travelled 18 inches (half of the maximum contemplated plate dimension). The

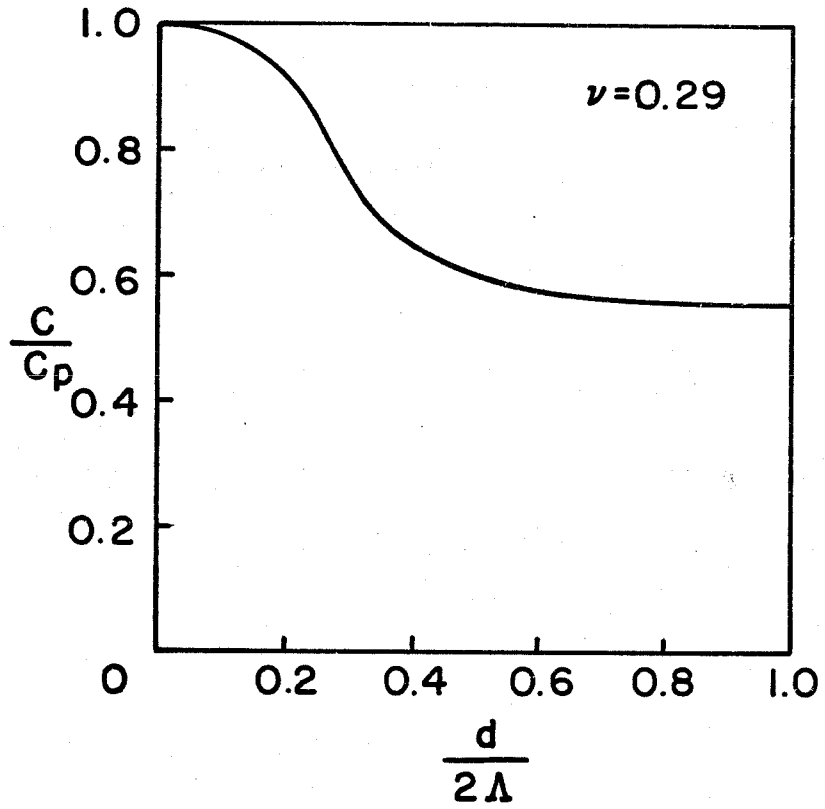

FIG. 4. Phase Velocity as a Function of Plate Thickness Divided by Wavelength

components were reconstructed taking into account the phase shifts and were then compared with the original wave forms. With the material properties of Homalite, a plate thickness of 3/16" and a simulated step with a risetime of 20 microseconds, the amplitude of the dispersed wave after 18 inches of travel was within 0.5 percent of the input wave amplitude.

The plate thickness of 3/16" represents a compromise of two conflicting constraints. As previously mentioned in a discussion of the electromagnetic loading principle, it is necessary for the width of the strip to be large relative to the separation of the two conductors. The other constraint is that a smaller thickness assures a smaller acceptable risetime from the viewpoint of wave dispersion. An additional consideration was the availability of material with minimal thickness variations.

With dispersion considerations requiring a thin plate and the method of loading requiring the application of stress to the faces of a long slender notch, the configuration of the specimen is essentially established. It remains to determine the dimensions of the notch and the lateral dimension of the plate. In the case of the lateral dimensions of the plate and the length of the notch, the characteristic time of the experiment and the plate velocity are the dominant factors. This is due to the requirement that the experiment is to represent crack behavior in an infinite domain. If a rectangular plate is assumed to have a notch cut from the edge at its midpoint and with a notch length of two thirds of the plate length, then there are two possible shortest paths for waves to

travel from the notch to a free edge and to return to the crack tip. If it is assumed that the desirable time is 225 microseconds and a maximum wave velocity of 81,000 inches per second, then a dimension of 9 inches from the crack tip to a free edge is sufficient.

D. Data Requirements

The objective of this research as previously stated was to correlate the onset of dynamic fracture with a loading history. The data that would be necessary to accomplish this correlation are records taken during each fracture experiment of the applied stress on the crack surface and the response of the specimen near the crack tip. With the aid of strain gages, a relationship between the current and the applied pressure was measured and used as a calibration of the loading device. It was therefore only necessary to record the current during each fracture experiment and not to strain gage-instrument each fracture specimen. A high speed framing camera capable of rates in excess of 100,000 frames per second was available for use with this experiment. By synchronizing the camera with the loading device, it was possible to correlate the load history with the specimen response and, in particular, to bracket the onset of crack propagation and determine crack velocities. At the rate of one frame every 10 microseconds, the experiment needed to have a duration of at least 50 microseconds and preferably longer in order to obtain adequate resolution of the onset of crack propagation. A duration of approximately 225 microseconds was chosen as a reasonable value and this period was used in sizing

the specimen and designing the pulse forming network. Details of the experimental configuration are contained in the next chapter.

4. DESCRIPTION OF EQUIPMENT

A. Specimen

The plate velocity for Homalite is approximately 81,000 in/sec. For an experiment with a duration of 225 microseconds, the simulation of an infinite plate would require that the crack tip be at least 18 inches from an edge, other than the crack surfaces, which could be the source of a stress pulse, or 9 inches from an edge that could reflect a pulse generated at the crack surface. This condition set the sizing requirements for the test specimen. A commercially available size that was closest to the minimum required was 30" x 24". Upon considering the various constraints such as photoelastic sensitivity, dispersion, alignment tolerances and commercially available sizes, a nominal specimen thickness of 3/16" was chosen. The actual thicknesses of the delivered articles varied from 0.1688" to 0.1846".

A slot 18" long and 0.05" wide was machined into each of the plates starting at the center of the 24" side. At the tip of the slot a "V"-shaped notch was introduced by means of a small triangular file. The angle of the "V" was 40 degrees. At the tip of the "V" a hairline fracture was produced by using a razor blade held in a tool, shown schematically in Figure 5, that permitted the gradual and controlled extension of the hairline fracture to the desired length. The crack extension beyond the copper strip was never less than 1/8" nor greater than 3/16" for any of the specimens tested. It should be noted that conditions at the crack tip such as residual stresses and crack tip radius due to "plastic"

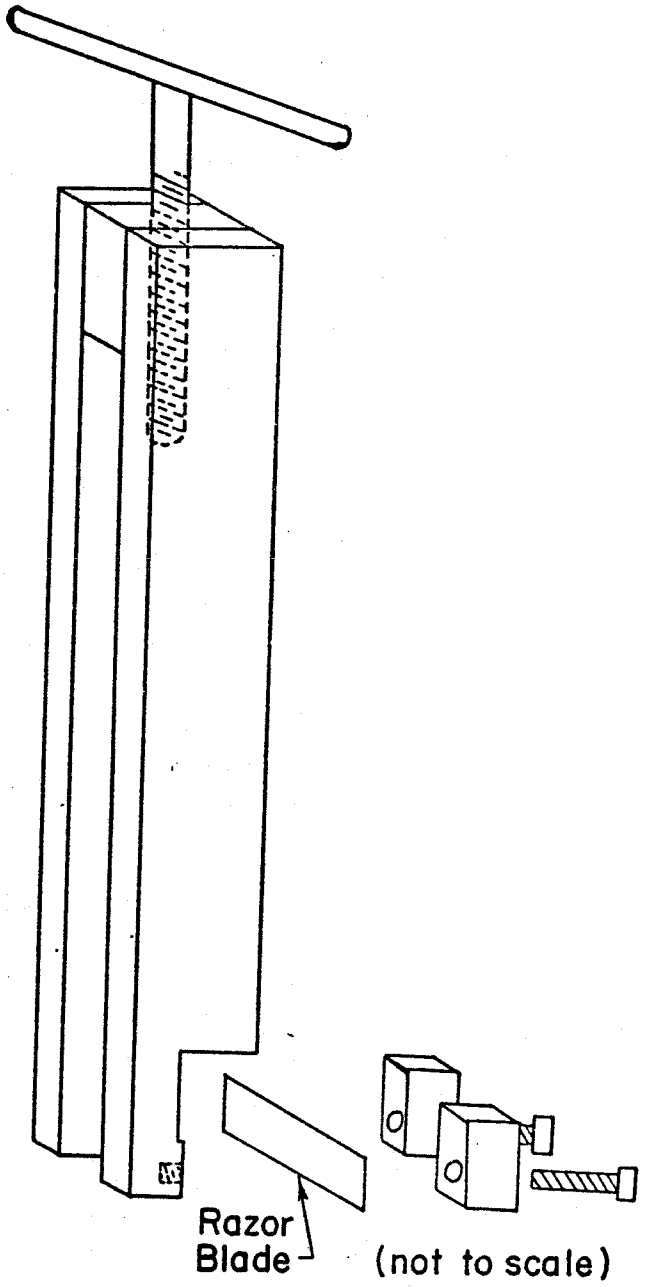

FIG. 5. Schematic of Tool to Create Hairline Fracture at Crack Tip

deformation could be highly significant. Care was exercised in making the hairline fractures in order to minimize, to the extent possible, variability of crack tip conditions in the unstrained state.

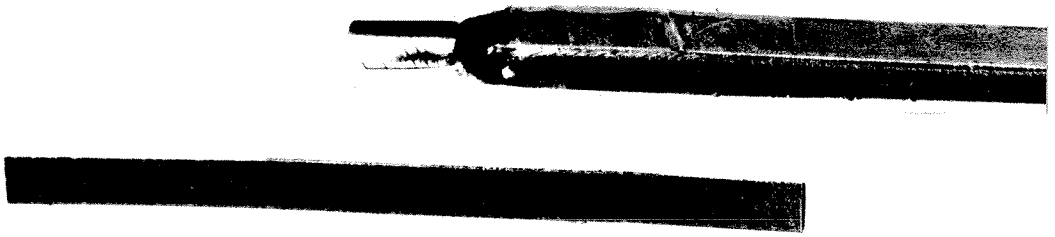

FIG. 6

Oblique View of Crack Tip

Figure 6 is an enlarged photograph of a representative crack tip region with a copper pressure strip in the slot. The dark rectangular object in the figure is a thin piece of brass which has the length of 1" along the longest side. In each of the fracture experiments, a reference length was attached to the plate within the field of view of the high speed camera recording the fracture behavior of the specimen.

B. Loading Device

The dynamic load was applied by a copper strip that was aligned along the 18" slot machined in the specimen. The strip was

double bent 180 degrees about a small (approximately 5 mill) radius of curvature which was then connected in series to a pulse-forming network.

The thickness of the copper strip was dependent upon the resistance heating that could be tolerated under the maximum current conditions. Conservative estimates of the temperature rise during the experiment were made by assuming that the copper strip was thermally insulated from its surroundings. It was found that the temperature rise during an experiment was inversely proportional to the square of the strip thickness. A limit was set for the temperature rise in order to assure that no unacceptable changes would occur in the elastic properties of the specimen material adjacent to the strip. For materials that can exhibit thermo-viscoelastic behavior, a sufficiently large temperature rise could, even at the proposed loading rates, be important. A review of the data on the viscoelastic nature of Homalite by Beebe [40] indicated that a change of 60 degrees centigrade would have only a marginal effect on the modulus at characteristic times of up to 200 microseconds. Preliminary experiments were run with copper strip thicknesses from 0.001" up to 0.050". The thickness that was chosen for the fracture experiments described in later sections was 0.020". This permitted a temperature rise of less than 50 degrees centigrade for the worst case.

The copper strips were slit by a commercial firm to the same width as chosen for the thickness of the plate (i.e., 3/16"). It was found that residual stresses in the sheets of copper caused

the slit strips to curl and warp. The strips were straightened by hanging a hundred pound weight on them for several hours which permitted the strips to creep straight. A mylar strip separated the two legs of the copper strip and provided insulation. The mylar could be slid easily but without much play between the doubled-up copper strip when it was bonded with a low-strength, water-soluble adhesive to the surfaces of the machined slot. The purpose of the adhesive was to assure firm contact between the strip and the specimen. When the bonding agent was absent, it appeared from strain gage records that the strip "rattled" about in the slot. This aspect is discussed further in the chapter on calibration.

Another basic element of the loading device is the pulse-forming network which furnishes the large currents through the copper strips. It was apparent from the start that a high-energy, low-inductance capacitor bank would be necessary to supply the current at the amplitude and with the response necessary for the experimental program. It seemed suitable to use an approach of forming the pulse similar to that used in radar applications [50] although the time frame and amplitudes are quite different. The approach was to use a number of identical capacitors that are connected by inductors of nearly equal inductances. For this study, nine Cornell Dubilier Type NRG-204 capacitors were used. They are rated at 15 micro-farads and 20,000 volts and had internal inductances of less than 0.06 micro-henries. The coils connecting the capacitors were made from number eight insulated copper wire wound on 6" diameter circular mandrels. Some difficulty was

encountered in constraining the coils to the prescribed circular shape. The current in the coils caused mechanical forces that tended to distort the coils. It was found that the mandrels, when combined with side-bracing members and reliance on the mechanical strength of the wire, were sufficient to maintain the structural integrity of the coils. Typically, for a low-resistance system, a set of nearly equal inductance coils placed between several capacitors will yield a ringing pulse that is nearly square, such as shown schematically in Figure 7.

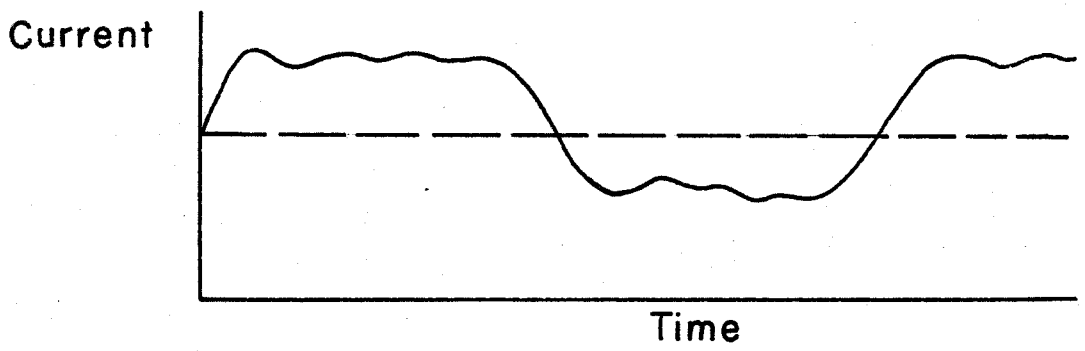

FIG. 7

The number of turns per coil was initially established using elementary electromagnetic principles and a simple mathematical model of the pulse-forming network. It was found that some empirically determined modification of the number of turns in the coils improved the current shape. The final number of turns for each

coil is shown in Figure 8. For the coil configuration described,

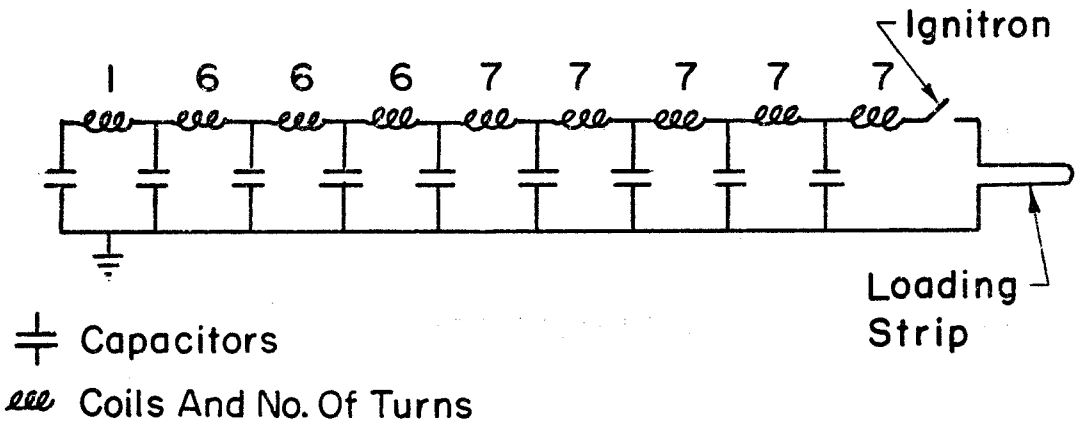

FIG. 8

Schematic of Pulse-Forming Network

seven turns corresponded to an inductance of approximately 180 micro-henries. The inductances of the other coils vary nearly directly with the ratio of the squares of the number of turns.

The fast switch for closing the circuit was an ignitron, General Electric Type GL-7703, which is a tube that contains a pool of mercury at its base. When a high voltage pulse from a triggering circuit is applied to an electrode near the pool, the mercury vaporizes and thereby closes the circuit between two other electrodes of the ignitron that are in turn connected to the capacitor bank. A drawback of the ignitron is that when current initially flows and when it reverses during the ring down of the capacitor bank, short bursts of electromagnetic noise are generated similar to those generated by arcs. The noise, however, did not prove to be a serious obstacle in this effort. A discussion

and a schematic of the ignitron triggering circuit are given in the thesis by Vlases [51].

C. Optical System

A high speed framing camera developed earlier at GALCIT [44] was used to record the motion of the crack tip during each of the fracture experiments. A schematic of the optical system and the camera is shown in Figure 9. The light source is shown at the lower left portion of the diagram. It consists of a 100 watt mercury arc lamp that is pulsed in order to achieve much higher intensities. The light first passes through a lens to achieve parallel light and then through a polaroid plate and a quarter wave plate. The parallel light beam continues through the specimen and a second set of quarter wave and polaroid plates which completes a circular polariscope configuration. The beam as it emerges from the polaroid plate indicated by the number two is at that point polarized. It is then condensed, passes through a Kerr cell* and encounters a final polaroid plate which has its axis perpendicular to the axis of the number two plate. When the Kerr cell is pulsed it effectively "uncrosses" the last two polaroid plates and allows the light to pass. The camera contains a circular track in which 10 feet of 35 mm film is placed. At the center of the circle formed by the film track is a rotating 45° mirror driven by an air turbine. When a 20,000

---

*A Kerr cell is a glass container filled with nitrobenzene liquid. Two metal capacitor plates are suspended in the nitrobenzene on electrodes which pass through the walls of the container. When a high voltage pulse is applied to the electrodes, the nitrobenzene becomes strongly polarized and acts like a quarter wave plate.

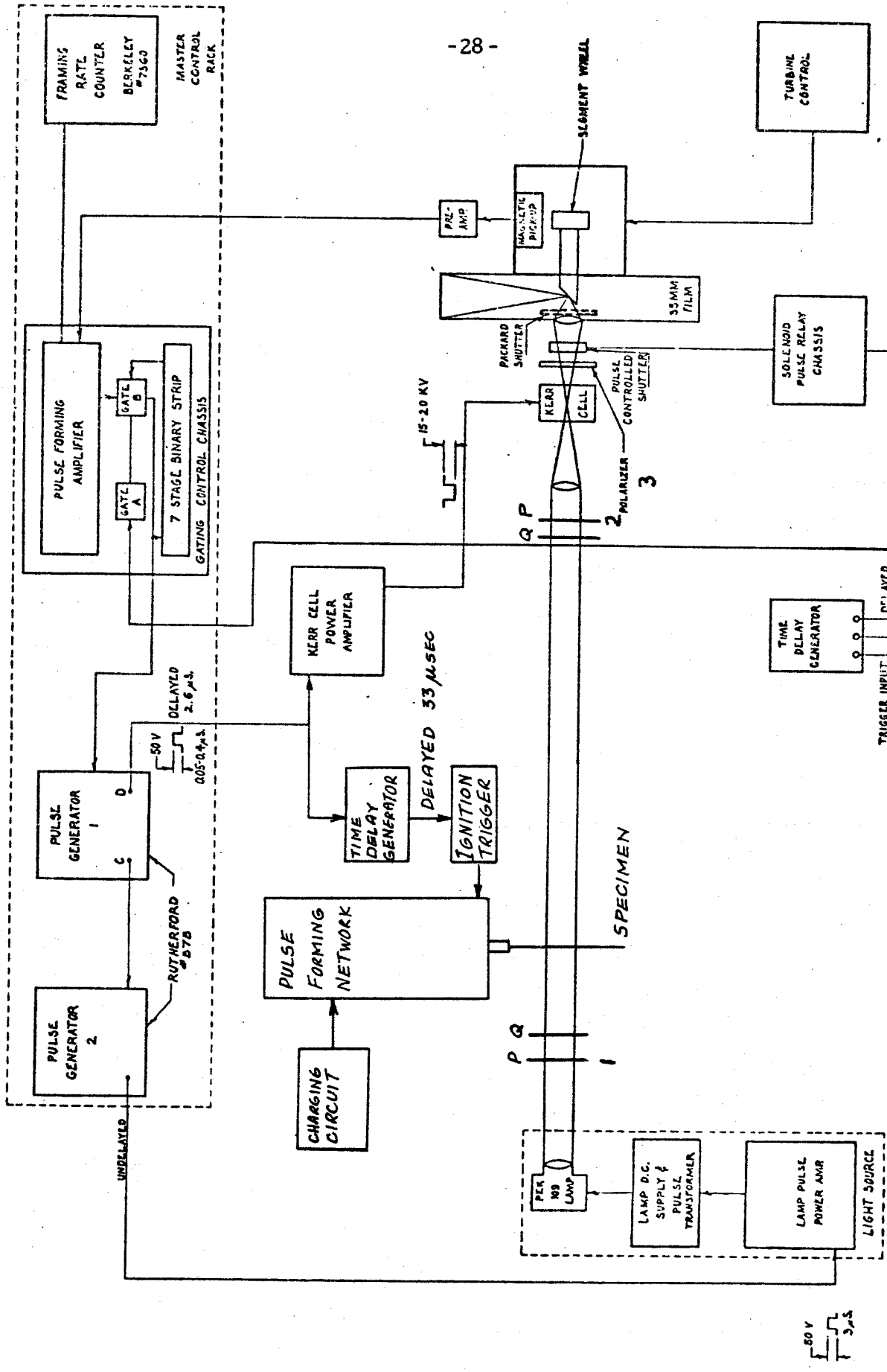

Figure 9. High Speed Camera System

volt DC pulse is applied to the Kerr cell, light passes through the No. 3 polaroid to the 45° mirror where it is deflected and forms a frame on the stationary film. During periods when the Kerr cell is not excited, only leakage light passes through polaroid No. 3. A magnetic pickup senses the position of the mirror and acts to space the frames properly by pulsing the Kerr cell and the light source. The mirror is rotated at a constant speed which is monitored on a Berkeley counter. The framing rate is continuously adjustable in the range of 10,000 to 100,000 frames per second. Exposure times can be adjusted from 0.05 to 0.40 microseconds. For all of the experiments reported in this thesis, the framing rate was 90,000 frames per second and the exposure time was 0.10 microseconds. Kodak Tri-X negative film and Acufine developer were used in these experiments.

D. Test Procedure

The equipment and specimen are shown in a typical test configuration in Figure 10. The cabinet at the far right of the photograph holds the pulsing amplifiers for the mercury arc lamp shown in the lower right foreground. The two large dark objects at the center of the photograph are the collimating lenses. The film track of the high speed camera is located at the upper left of the photograph. At the lower left is a portion of the case that holds the capacitor bank. The tall cabinet immediately to the right of the film track contains the charging circuitry for the capacitor bank and the triggering circuit for the ignitron (not shown in Figure 10). The camera controls and pulsing circuits and oscilloscopes that

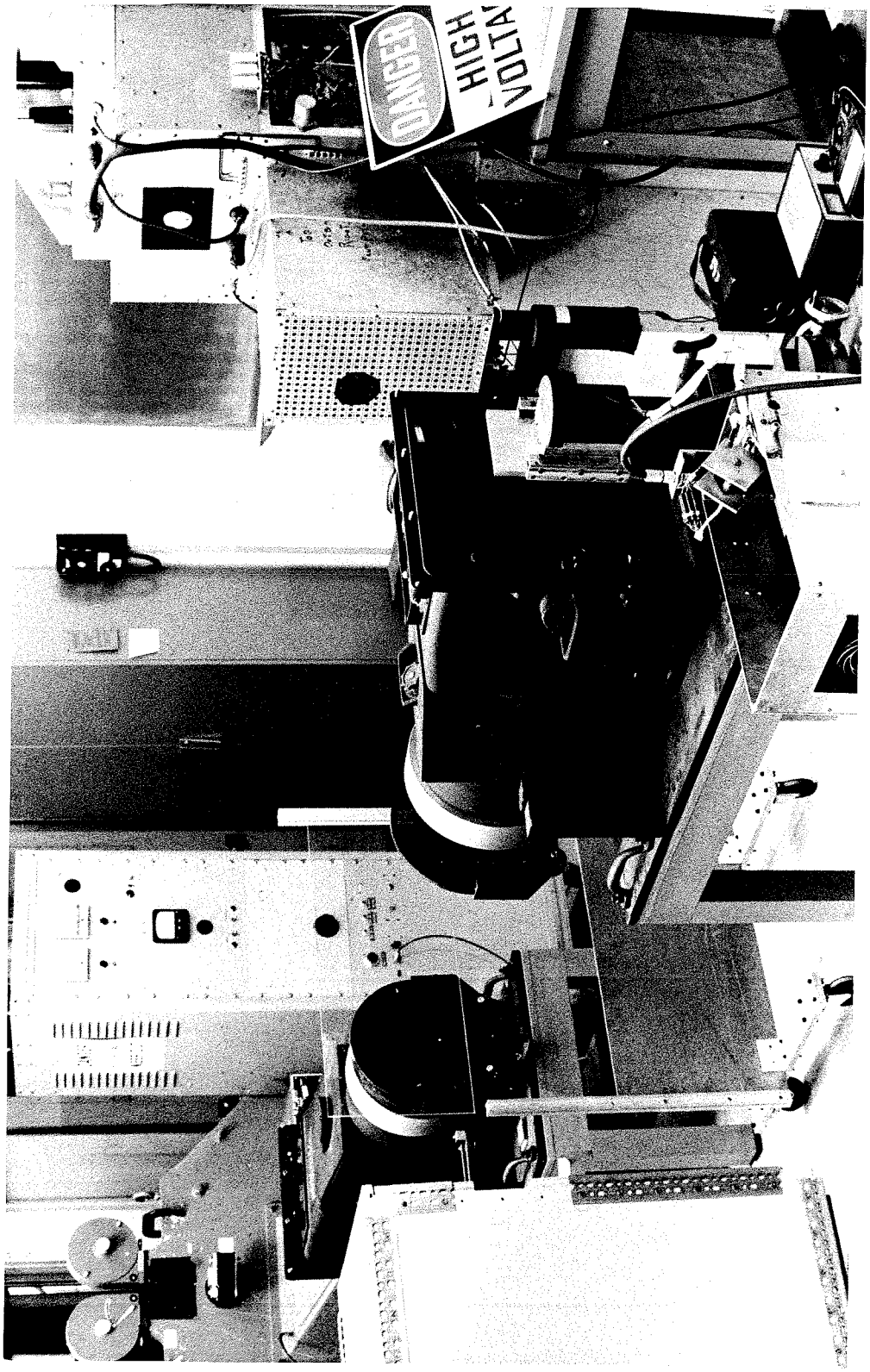

FIG. 10. High Speed Camera and Electromagnetic Loading Device

are used during a fracture experiment are located in an adjacent room. These were placed at a distance from the loading device in order to minimize electromagnetic interference problems.

A closer view of the specimen is shown in Figure 11. The 30" dimension of the specimen is along the top edge as shown in the figure. The copper strip is in the 18" slot and connected to the capacitor bank by mechanical clamps that facilitated easy replacement of the specimen. At the top front end of the container is a portion of the Rogovski coil that was used to measure the current. A more complete view of the Rogovski coil is shown in Figure 12, which also shows the ignitron, two of the coils and two of the capacitors that are part of the network that forms the current pulse for the loading strip. The ignitron is supported by a broad strip of copper attached to the front capacitor, and is shown at the center of the photograph. The light-colored square above the ignitron is mylar insulation to prevent arcing.

A typical dynamic fracture experiment proceeded as follows. After the equipment had been allowed to warm up and was checked for proper settings, the capacitor bank was charged to at least 2,000 volts but less than 20,000 volts. The voltage level for any particular fracture experiment determined the current in the strip which in turn determined the level of stress applied to the crack surfaces. Air pressure was then applied to the turbine that was attached to the rotating mirror in the camera. The amount of pressure to the turbine determined the angular rate of rotation and the corresponding framing rate which was displayed on a Berkeley

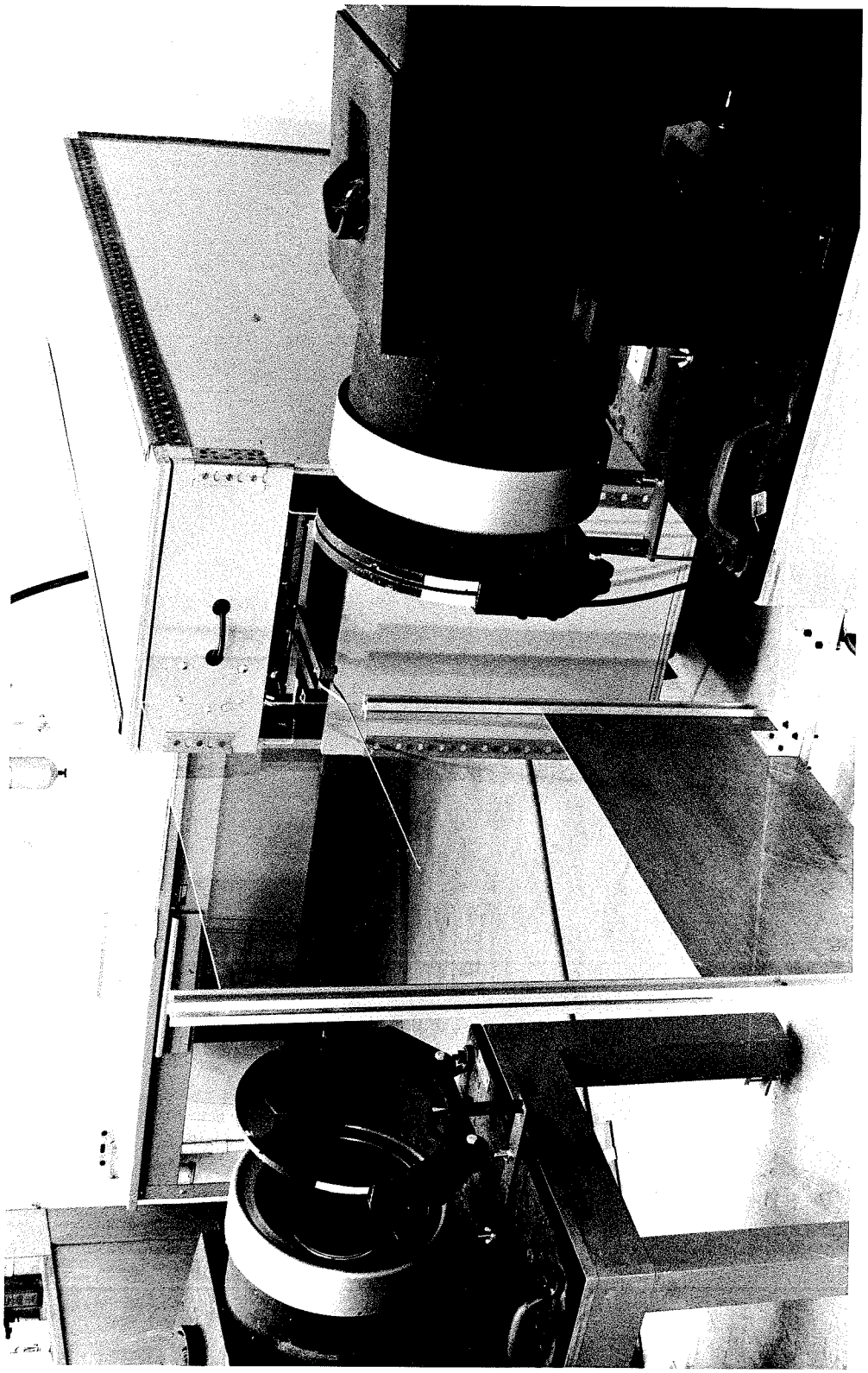

FIG, 11. Test Specimen and Electromagnetic Loading Device

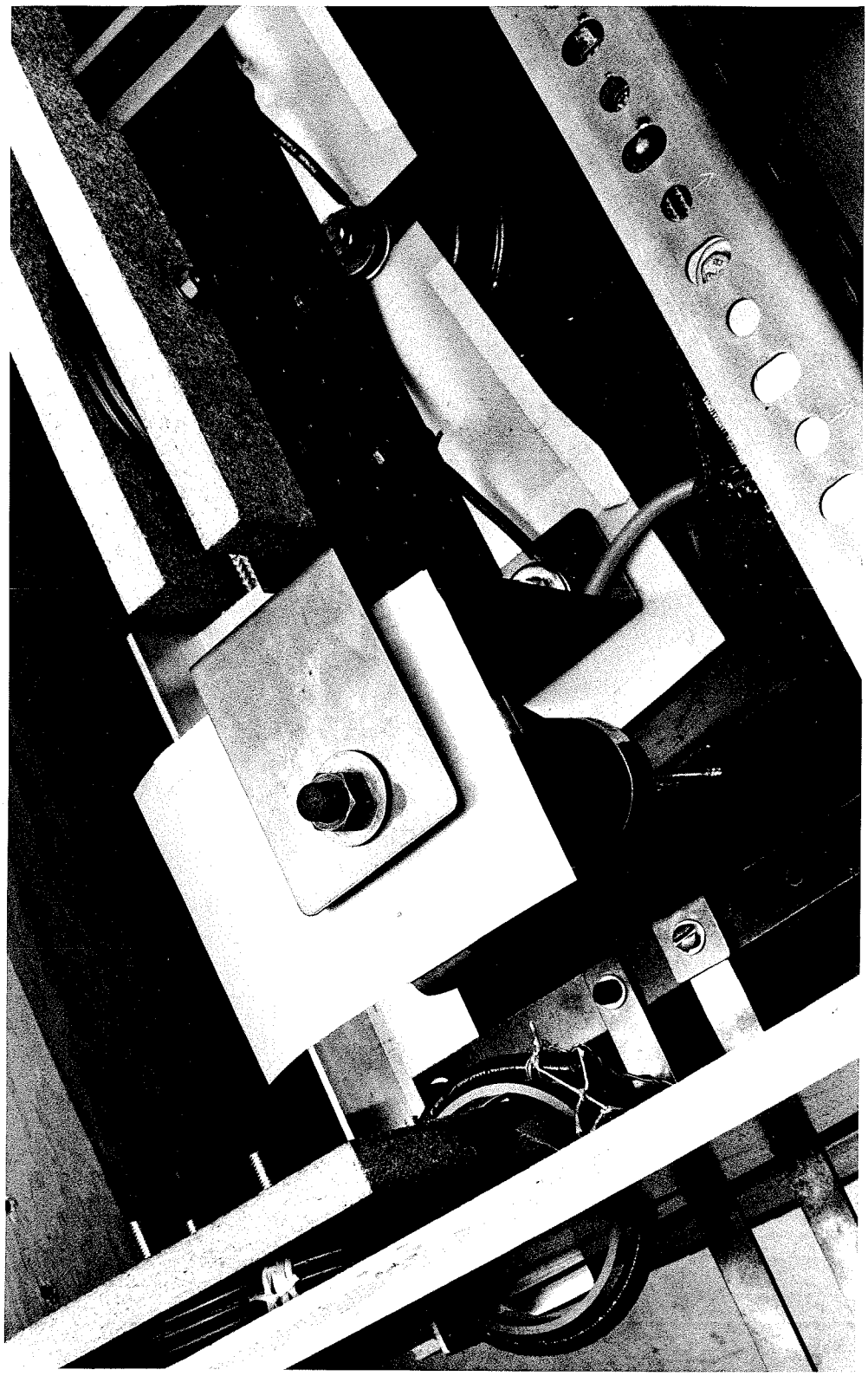

FIG. 12. Ignitron and a Segment of the Pulse-Forming Network

counter. The air pressure was manually adjusted until the framing rate reached 90,000 frames per second. When the turbine reached the proper speed, a triggering signal was sent to the camera master controls which pulsed the Kerr cell and light source amplifiers, and to an oscilloscope that was to record the current as a function of time. The pulses sent to the Kerr cell amplifier were also connected to a time delay generator set for a 33 microsecond delay. The output of the time delay generator activated the triggering circuit of the ignitron which is the switch for the pulse-forming network connected to the pressure strip. Thus the camera and the loading device were synchronized and the loading began as the fourth frame was being exposed.

During the experiment, the Rogovski coil, which was attached to the capacitor bank container, generated a voltage which was proportional to the time rate of change of the current in the strip. This voltage was integrated by an RC integrator and was recorded by the oscilloscope that had been previously triggered. A polaroid photograph was made of the record. This record was then used to determine the stress applied to the crack surfaces as a function of time by means of an empirical relationship discussed in the following chapter.

The master control of the high speed camera pulsed the Kerr cell and light source exactly 64 times, which generated that number of frames at 11 microsecond intervals. The developed negative was used to determine crack extension as a function of time and to determine the onset of crack propagation.

5. CALIBRATION OF EQUIPMENT

A. Rogovski Coil Calibration

Details on the construction and constraints applicable to a Rogovski coil are contained in [52]. The application of the coil in the present work was to generate a voltage proportional to the time rate of change of current in the loading strip. This voltage was integrated by means of an RC integrator and a signal proportional to the current was available for display on an oscilloscope. The Rogovski coil and integrator were calibrated by generating a known current and correlating the current with the recorded output. If all but one capacitor is removed from the pulse-forming network, the remaining circuit is then an RLC series circuit. The single capacitor of the circuit was charged to a known voltage and when the ignitron was activated, a decaying sinusoidal signal was recorded. From elementary analysis, it can be shown that the first peak of the current is given by:

$$I_{(T/4)} = V_o\, C\left(\frac{2\pi}{T}\right)\left(\frac{A_3}{A_1}\right)^{\frac{1}{4}} \qquad (3)$$

where T is the period of oscillation, C is the capacitance, V_o is the initial voltage on the capacitor, and A_3/A_1 is the ratio of two successive peaks of the same polarity. The period T and the ratio A_3/A_1 can be found from the trace on the oscilloscope. Figure 13 shows the calibration traces for 5,000 and 10,000 volt charges on a 14.5 micro-farad capacitor. A calibration factor can then be found by dividing the quarter period current by the corresponding

recorded output voltage. For the configuration used in the fracture experiments, the calibration factor was 24,815 amperes per volt of the integrated signal.

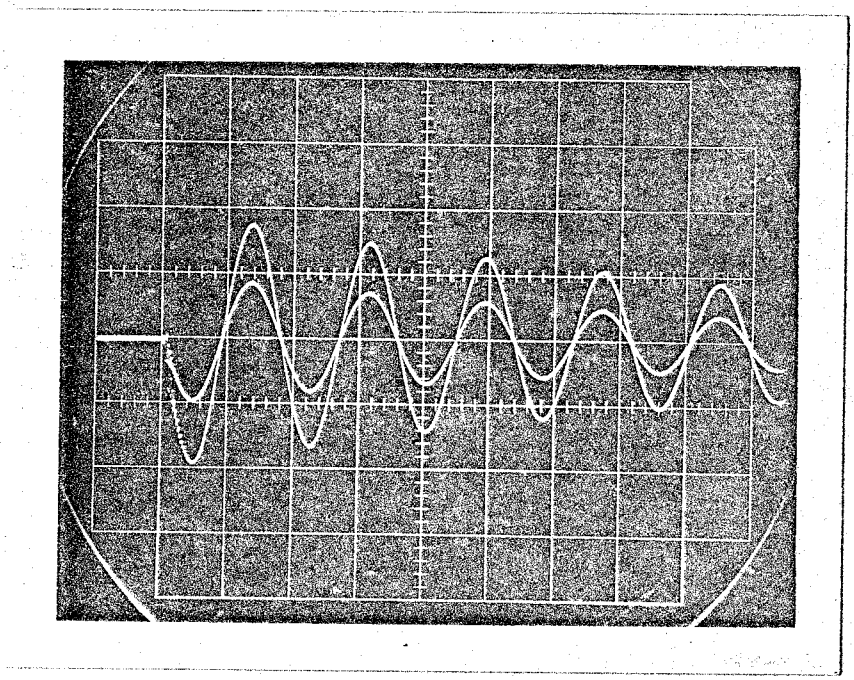

Horizontal Scale: 50 μsec/div
Vertical Scale: 0.2 v/div

FIG. 13

Calibration Traces for the Rogovski Coil

B. Calibration of the Loading Device

The relationship between the pressure applied to two parallel flat strips when they are close together and conducting current in opposing directions was given in Eqn. (2). In dimensional form for the case when the width of the strips is set at 3/16", Eqn. (2) has the form:

$$P = 4.04\ 10^{-6}\ i^2 \qquad (4)$$

where i is in amperes and P is in pounds per square inch.

The approach taken in the experimental calibration of the loading device was to attach semiconductor strain gages to plates of Homalite and correlate the current from the Rogovski coil and the stress determined from the output of the strain gages. It was immediately apparent that the magnetic fields created by the high currents in the loading strip and in the pulse-forming network would generate considerable interference in the strain gage circuits and loads. Two techniques were used to counter this problem. It was found that placing large thin sheets of aluminum about the pulse-forming network considerably reduced the noise picked up in the strain gage circuitry. It had the added effect of eliminating apparently spurious signals that were causing erratic behavior of the control circuitry for the high speed camera.

The second technique involved the use of a Wheatstone bridge and was highly effective in reducing the noise level. The Wheatstone bridge [53] is frequently used to determine the change in resistance which a gage undergoes when it is subject to a strain. The bridge may be used as a null balance system whereby the strain is proportional to a voltage excursion from a nominal zero datum. The principle employed to reduce the noise is very similar to that used in the temperature compensation of strain gages; namely, placing an identical dummy gage physically near the active gage so that both experience the same environment and unwanted effects common to both are cancelled by the null balance feature.

A typical strain gage arrangement that was used for some

of the calibration data is shown in Figure 14. The gages are matched BLH semiconductor strain gages, type SPB3-06-12. The gage length is 0.06" and the basic gage factor and resistance are typically 108.5 $\pm$ 2% and 128.3 $\pm$ 1% ohms. The gray rectangular object to the left of the gages is a one-inch reference length. There are actually three gages shown in the figure. There is a dummy gage mounted on a thin piece of black plastic and two gages bonded back to back on opposite sides of the calibration specimen.

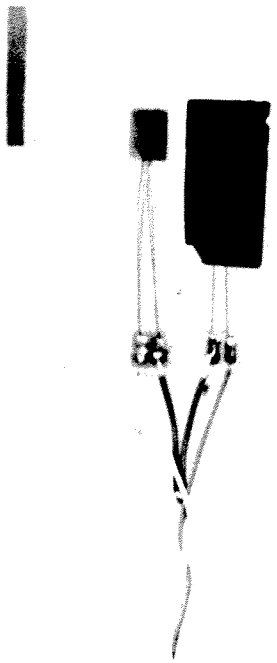

FIG. 14

Photograph of Strain Gage Configuration

Uncracked Homalite plates were used for calibration where the load was applied to the 30" long edge as shown in Figure 15.

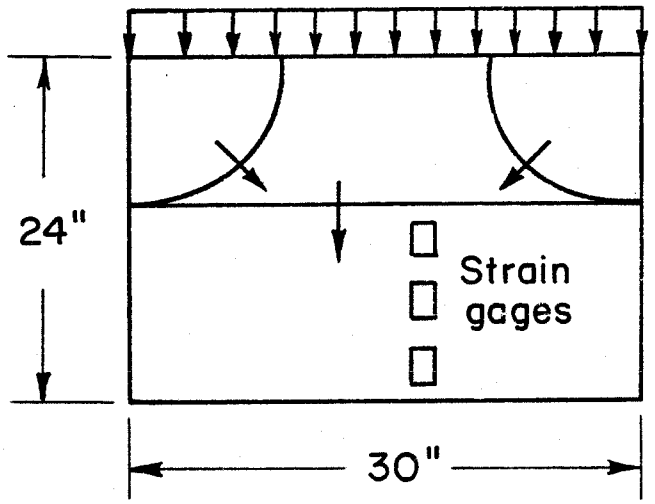

FIG. 15

Uncracked plates were used for calibration in order to have a longer strain record than could be achieved from the 18" notched specimen. It was found that the current shape for the 30" strip could not be distinguished from the 18" strip for the same voltage on the capacitor bank to within the resolution of the oscilloscope trace. This was reasonable because the capacitance, inductance, and resistance of the strip were quite small compared to that which was integrally associated with the pulse-forming network.

During preliminary attempts at calibration, it was found that the measured strain differed in shape from that of a square pulse with a finite rise time. It appeared that a high frequency

component was superposed upon the expected shape, as can be seen in Figure 16. The top two traces are the integrated output of the Rogovski coil with a slight shift in the zero position for two separate loading histories resulting from the same initial capacitor voltages. The similarity of the two traces is typical of the repeatability of the loading device.

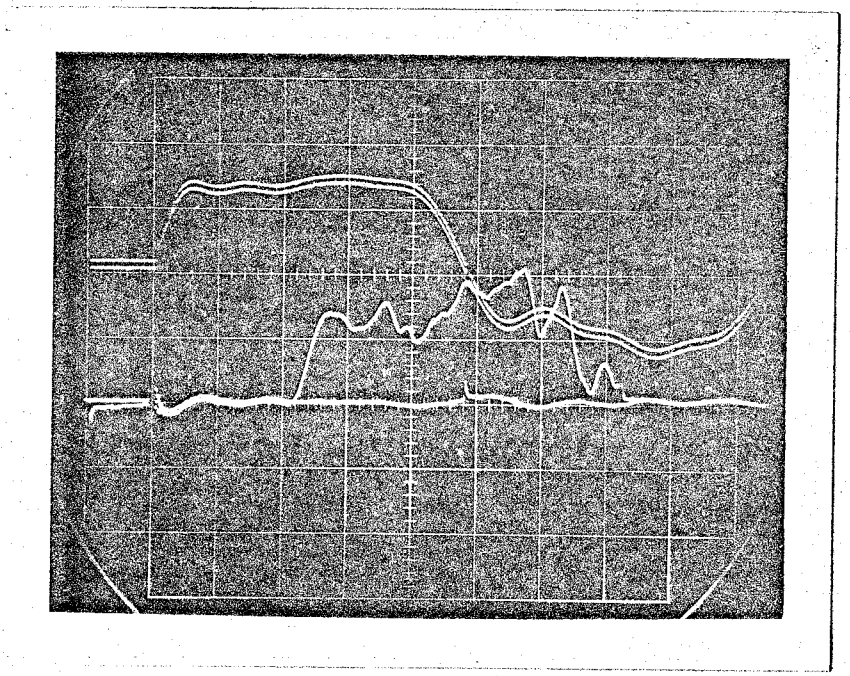

Horizontal Scale: 50 μsec/div
Vertical Scale Upper trace: 4960 amps/div
Lower trace: 43 psi/div

FIG. 16

Current and Strain Gage Traces for Non-Bonded Pressure Strip

The output of the Wheatstone bridge was also recorded except that for one test, power was supplied to the bridge and for the other the power was disconnected. The latter case was run to determine the noise picked up by the strain gages and leads in the presence of magnetic fields. This is shown by the lower nearly horizontal trace.

The high frequency components were apparently due either to the copper strip repeatedly hitting and rebounding from the plate edge or to the presence of higher modes. It was found that when the strip was bonded to the edge of the plate with "Elmer's Glue-all," repeatable and consistent strain records were obtained. Silicon grease was tried as a contact agent and although it caused improvement, it did not yield consistent results. Thus for the calibration and for all of the dynamic fracture experiments reported here, the loading strip was bonded into place.

Figure 17 is a polaroid record of four traces taken during a typical calibration of the loading device. The top two traces (without the zero offset) record the current history and the bottom two represent the voltage measured across the Wheatstone bridge for cases with and without power. The lower trace is a measure of the noise and as before is quite small. There are, however, two excursions (at 50 and 300 microseconds) from a nominally zero value. They occur when the ignitron is triggered and an arc is formed to allow current to begin to flow and again when the current is extinct and then reverses as an arc forms to allow the current to flow in the opposite direction.

The difference between the bottom two traces is a measure of the strain. It can be seen that there is no strain until 55 microseconds after the load is applied to an edge. This delay is the time required for the stress pulse to travel a distance of 4.5" to the strain gages at the plate speed. The value of the plate speed (81,000 in/sec) was confirmed on other specimens that had strain

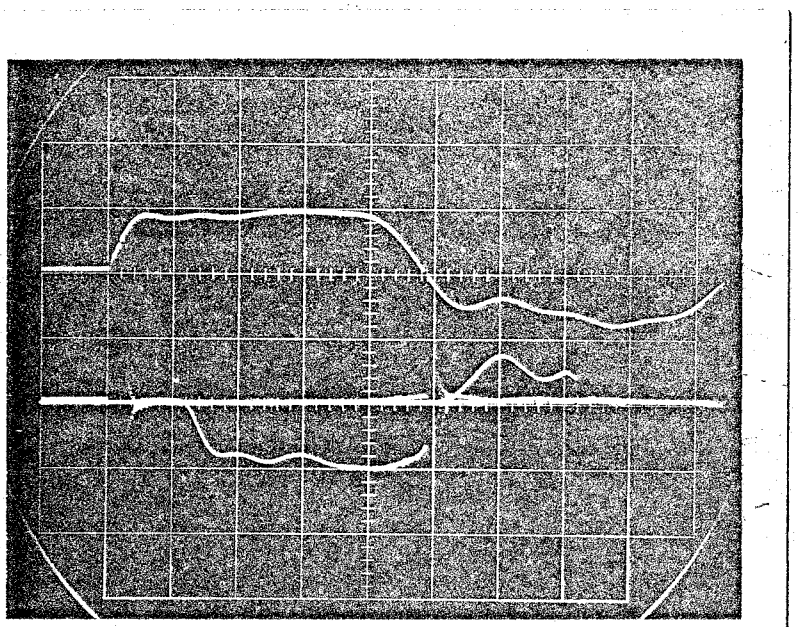

Horizontal Scale: 50 μsec/div
Vertical Scale Upper trace: 4960 amps/div
Lower trace: 43 psi/div

FIG. 17

Typical Current and Strain Records

gages at three, six, and nine inches from the leading edge. With the measured plate velocity, a density of 0.00434 lb/in^3, and using a value of Poisson's ratio taken from other investigations [6, 40], the modulus effective at wave propagation loading rates was found to be 649,000 psi. This compares to a 540,000 psi value under static conditions. The difference between the dynamic and static moduli is indicative of the viscoelastic nature of Homalite which is discussed by Beebe [40]. For the rates of loading applicable to the experiments described in this thesis and at room temperature, Beebe's data indicate that a nearly constant value of the modulus can be expected.

To illustrate the sensitivity of the physical configuration of the strain gage leads, let us consider an alternative to the one shown in Figure 14. An alternative configuration was used in which the ground lead was connected directly to one of the terminals instead of to a "Y" formed wire and a short lead then connected two adjacent tabs as shown in Figure 18.

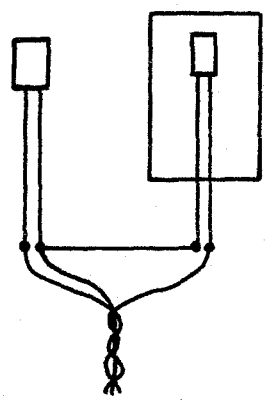

FIG. 18

An Alternate Configuration of the Gage Leads

An experiment with the alternate wiring was performed and the resulting trace is shown in Figure 19. Unlike the results shown in Figure 17, the trace for the case of no voltage across the bridge is large relative to the strain trace. It is, however, still true that the strain is proportional to the distance between the bottom two traces, since the only difference between the two cases is that the noise common to one set of traces is more than the noise common to the other set.

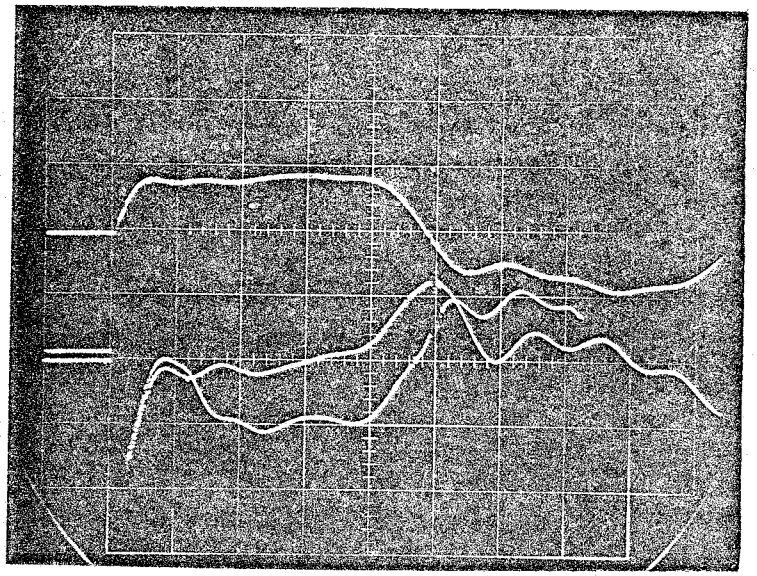

Horizontal Scale: 50 μsec/div
Vertical Scale Upper trace: 4960 amps/div
Lower trace: 43 psi/div

FIG. 19

Strain Gage Traces where the Electromagnetic Noise is Significant

The two strain measurements discussed above involve the dummy gage attached to a small separate piece of plastic and the gage attached to one side of the specimen. It follows that the strain readings obtained in this manner would include axial and any bending components that might exist. Bending components could be introduced by misalignment in the loading strips resulting in a net moment. In order to assess this possibility, the strain gage which was bonded on to the specimen shown in Figure 15 on the opposite side of the specimen was substituted for the dummy gage on the

separate piece of black plastic. In this case, if the leads are symmetric then the signal recorded would be proportional to twice the asymmetric components. The specimen was loaded twice as previously described and the result is shown in Figure 20. In this case, as it was in similar tests, the asymmetric components of strain were less than 10% of the axial strains for the period prior to the arrival of the unloading waves.

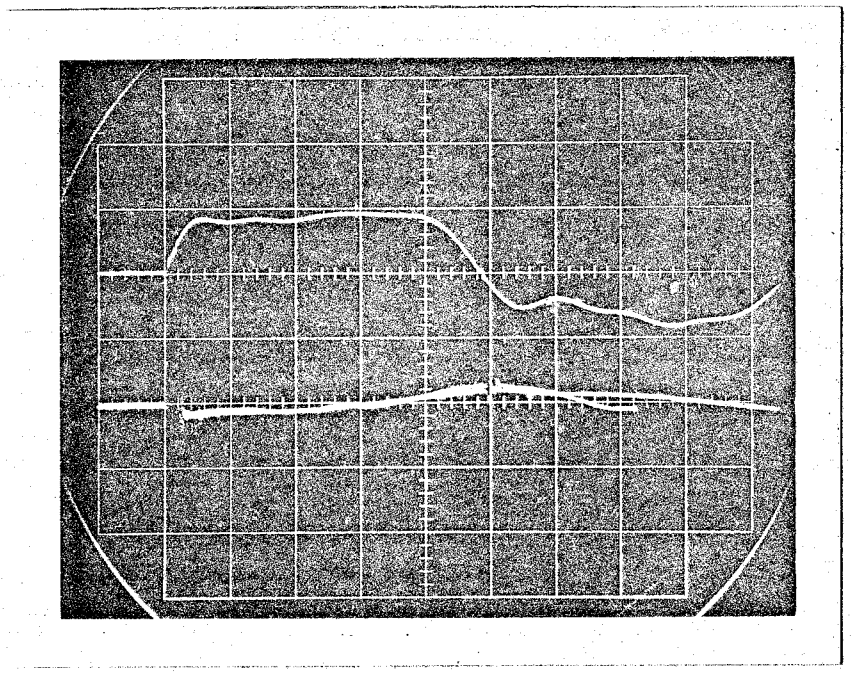

Horizontal Scale: 50 μsec/div
Vertical Scale Upper trace: 4960 amps/div
Lower trace: 43 psi/div

FIG. 20

Strain Gage Trace of Asymmetric Strain Components

The voltage applied across the gages was on the order of two volts. This is a relatively high value from considerations of heat dissipation of non-conductive plastic-like materials. The high voltages were needed, however, to give output signals that were

large relative to noise. In order to avoid heating the gages and thereby changing the specimen modulus, the voltage across the bridge was pulsed for 400 microseconds. The result of this pulsing can be seen in the previous four photographs in that the strain traces seem to discontinue at 400 microseconds. At that point, the trace drops to zero corresponding to zero bridge voltage, and the two traces superpose.

The three photographs in Figures 17, 19, and 20 show traces for the strain gage at $4\frac{1}{2}$" from the loaded edges. Data were also taken from Celesco strain gages, P01-05-500, which were placed 3, 6, and 9 inches from the loaded edge. The gage factors for these gages were determined empirically by cutting a strip out of the test specimen (plate) containing the three gages and then calibrating with known strains. A polaroid record of three different tests from a Celesco gage nine inches from the loaded edge is shown in Figure 21. The top three traces represent the current for 4,000, 5,000, and 6,000 volt charges on the capacitor bank. The corresponding strain records also appear but without the zero power reference. This trace illustrates that stress wave rise-time is independent of load level as expected and that while the current varies linearly, the strain varies with the square of the initial voltage on the pulse-forming network. Comparing the strain traces of Figure 22 with those of Figure 17, it is apparent that the delay associated with the stress wave traveling 9" is twice that for traveling $4\frac{1}{2}$" while the risetime is essentially unchanged.

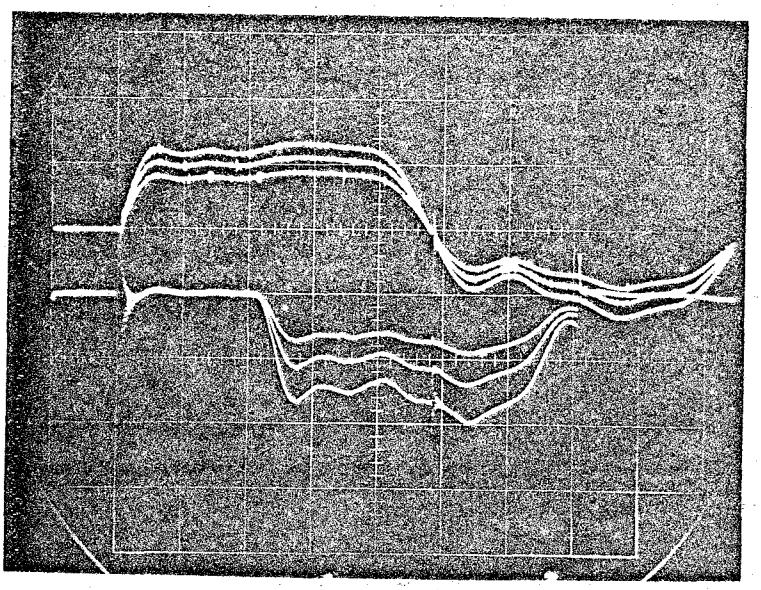

Horizontal Scale: 50 μsec/div
Vertical Scale Upper trace: 4960 amps/div
Lower trace: 59 psi/div

FIG. 21

Current and Strain Traces for a Family of Current Levels

It was expected that some dispersion and attenuation would occur as a pressure pulse developed by the electromagnetic device traveled in the plate. Since it was not possible to record the strain from gages located closer than approximately 3" to the loaded edge of the plate (because of electromagnetic interference), during the time interval $0 < t < 25$ μsec, compensation was employed to correct the strain gage measurements. To accomplish this, gages were placed at three- six- and nine-inch distances from the loaded edge and their responses were compared at various load levels. Figure 22 shows the stress for each of the gages normalized by the corresponding stress at the three inch gage. The results indicate that

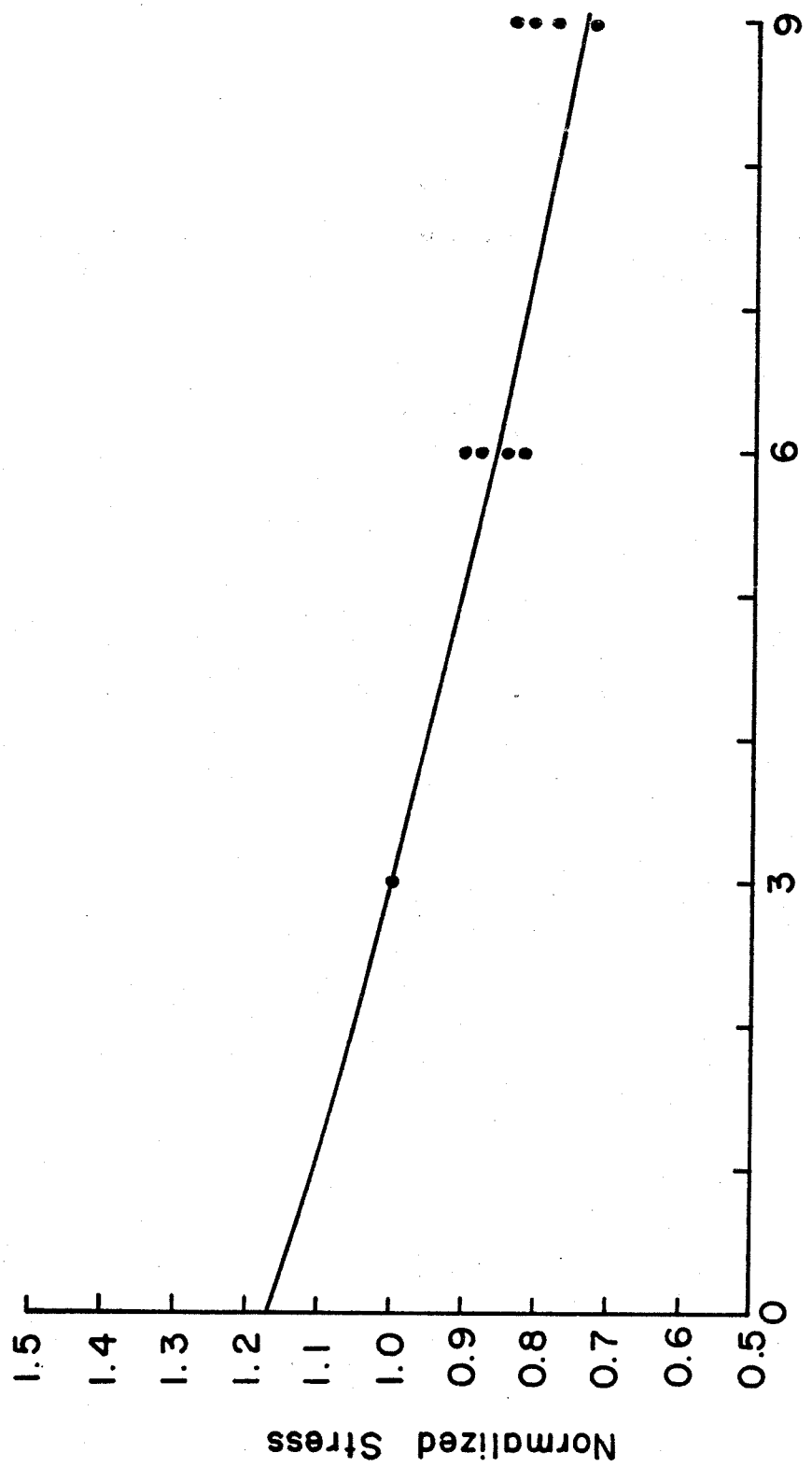

FIG. 22. Attenuation of the Stress Wave with Distance Traveled

attenuation of the signal is indeed present. It has been shown, using modeled and measured material properties, that a pulse traveling in a viscoelastic material at the glassy velocity (i. e., the velocity associated with glassy modulus) will decay exponentially with time and distance [61, 62, 63, 64, 65]. Thus an exponential curve was fit to the data shown in Figure 22 and extrapolated to yield the expected value of applied stress on the boundary.

The stress, as determined from the BLH strain gage located $4\frac{1}{2}$" from the loaded edge, is shown plotted (plot #1) against the square of the measured current at various load levels in Figure 23. When the compensation for attenuation described in the last paragraph is applied, the corresponding curve for the stress applied at the loaded edge of the plate is found to be the one labelled "2". The third curve (labelled "3") of Figure 23 represents the theoretical expression given by Eqn. 2 for the ideal case. The empirically determined factor relating the stress to the square of the current is 3.15×10^{-6}, which is 78 percent of the value indicated in Eqn. 2.*

The subsequent chapter contains the results of 11 dynamic fracture experiments. In these tests, the Rogovski coil was used to measure the current which, combined with the empirically determined factor, established the time-dependent tractions applied to the crack surfaces.

---

*The 20% deviation from the expected behavior was discussed with Prof. R. Langmuir at CIT. Corrections on the order of 5% are needed to correct for deviation of the loading device from the ideal geometry underlying Eqn. 2. Since the interest here was on generating a known pressure and not in electromagnetic theory, the calibrated results were used without further work.

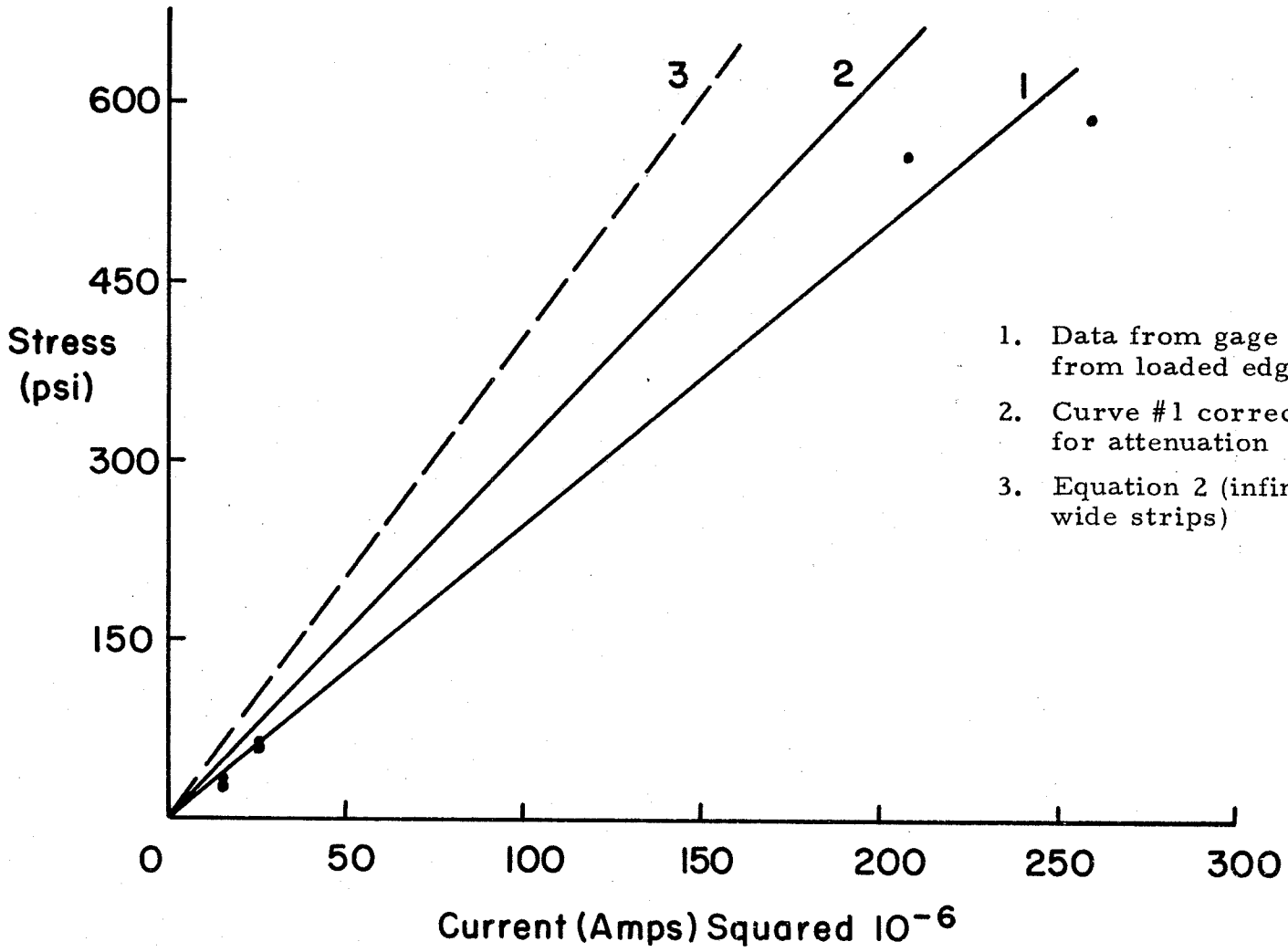

FIG. 23. Electromagnetic Loading Device Calibration

6. EXPERIMENTAL RESULTS

Ten dynamic fracture experiments were performed in accordance with the previous procedure. From the high speed cinematographs, the crack extension as a function of time, the amount of time that had elapsed before each crack had begun to extend from its original length, and the velocity and acceleration of each crack were determined. From the stress and current calibration described in the previous chapter, the stress applied on the crack boundary was determined as a function of time for each experiment. These data were then used in the analysis of the fracture process.

The field of view on the cinematograph was circular with a 7" diameter. The undisturbed crack was aligned along a diameter with its tip located approximately 2" into the field of view. This permitted a view of the crack tip region and the observation of the crack as it ran for the remaining 5" before the tip left the field of view. Although a circular polariscope was used in conjunction with the high speed camera, the quality of the photoelastic fringes did not permit quantitative determination of the stress field. The fringes did, however, aid in following the crack tip as it progressed.

The current trace for a typical experiment is shown in Figure 24. The trace has the same shape as those discussed in the section on calibration and the other experiments in the test series. The current of the local maximum occurring 25 microseconds after triggering the loading device is 14, 400 amps, which corresponds to 454 psi being applied to the crack faces. Figures 25a and b contain 12 prints, made from the high speed camera negative, and show

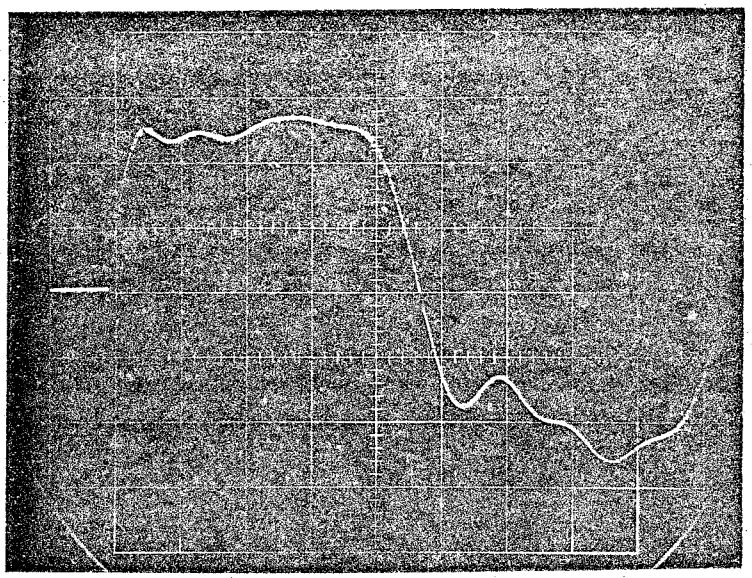

Horizontal Scale: 50 μsec/div
Vertical Scale: 4960 amps/div

FIG. 24

Current Trace from a Typical Fracture Experiment

the response of a crack at 11 microsecond intervals during the experiment discussed in connection with Figure 24. The small rectangle shown in the prints is a thin brass strip used as a reference length (1" long on its longest side). Two faint lines also appear in the prints. These are reference scratch marks made on the plate and, if extended toward the crack, would intercept the crack tip and the outside radius of the copper strip, respectively. The initial frame in the series shown in Figure 25a is the plate in the unloaded state. Subsequent frames have dark regions which are indicative of the stress waves that propagated away from the crack region.

The 35 mm film from this and the other experiments were

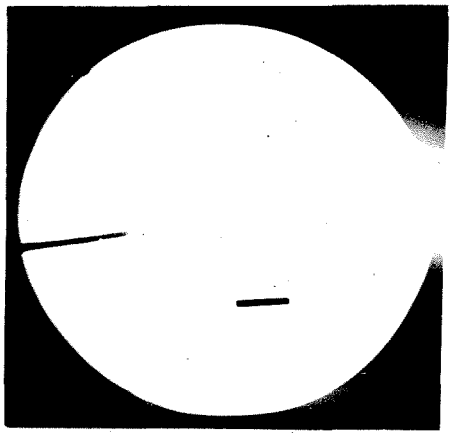

0 μsec

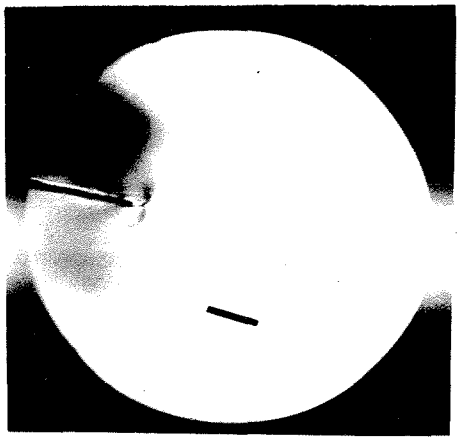

33 μsec

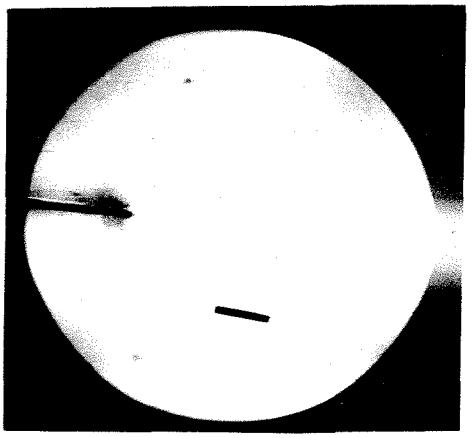

11 μsec

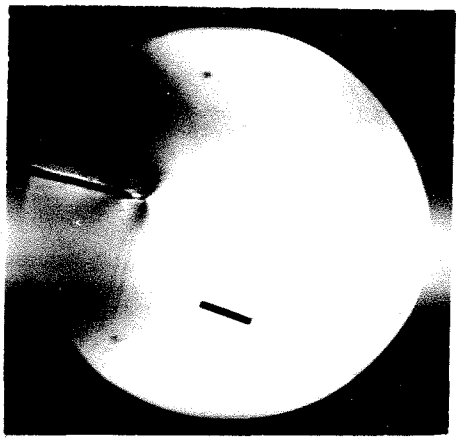

44 μsec

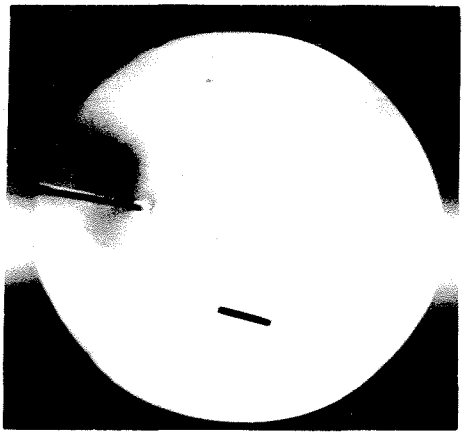

22 μsec

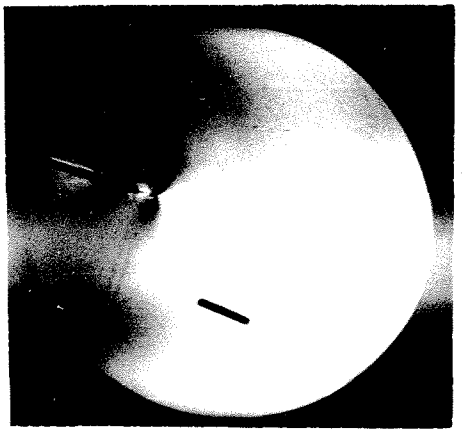

55 μsec

FIG. 25a. High Speed Cinematographs of a Fracture Experiment

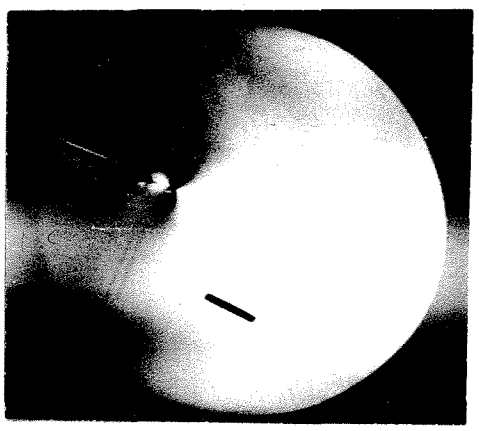

66 μsec

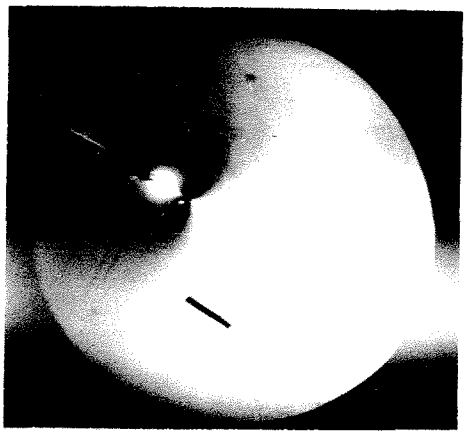

99 μsec

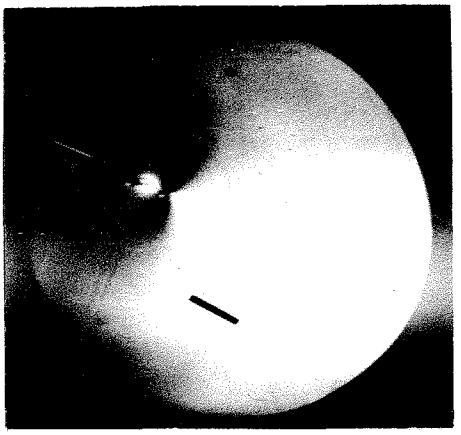

77 μsec

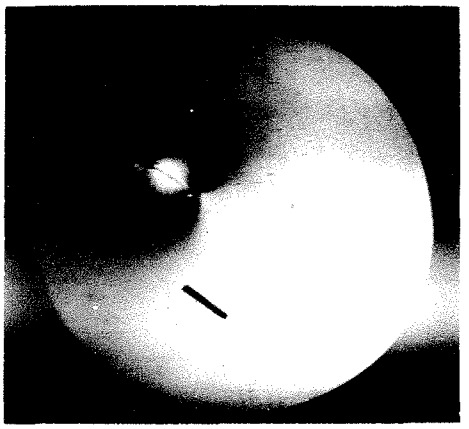

110 μsec

88 μsec

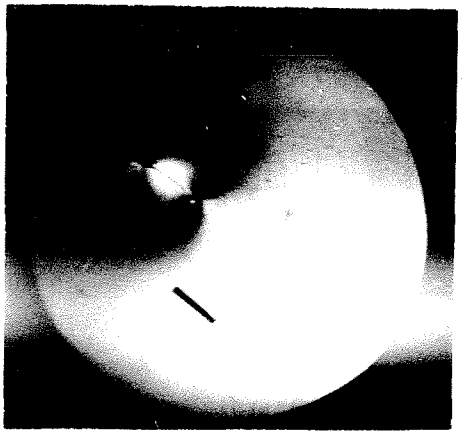

121 μsec

FIG. 25b. Continuation of High Speed Cinematographs

displayed on a Recordak viewer that allowed a seventy-fold lineal magnification. That enlargement corresponded to an image at twice the real scale. Measurements were made from the initial location of the crack tip to its location as shown in each photograph for each specimen. It was estimated, after a series of repeated measurements of initial crack lengths displayed on the Recordak viewer, that the error in measurement was $\pm$ 0.03".

Figure 26 is a plot of the crack extension as a function of time for each of the experiments. Each curve is composed of between 20 to 50 points, which for reasons of clarity in plotting, have been omitted from the figure. The curve corresponding to the highest current in the copper strip, and hence the highest applied stress, is the curve at the far left of Figure 26. The curves progressively to the right correspond to decreasing values of the current flowing in the loading strips. Two of the curves plotted in Figure 26 are discontinuous. The omitted sections were due to a design quirk in the high speed camera which randomly causes loss of 8 frames. The data lost from these two experiments were not critical with respect to the intended purpose of determining the onset of crack propagation and, therefore, the residual data from the affected experiments were included in this account. The terminal crack velocities ranged from 10,600" per second to 17,500" per second and show a consistent increase with the increasing level of the boundary loading. Previous investigators using quasi-static loading reported terminal crack velocities of 15,300" and 15,000" per second for Homalite [4, 40].

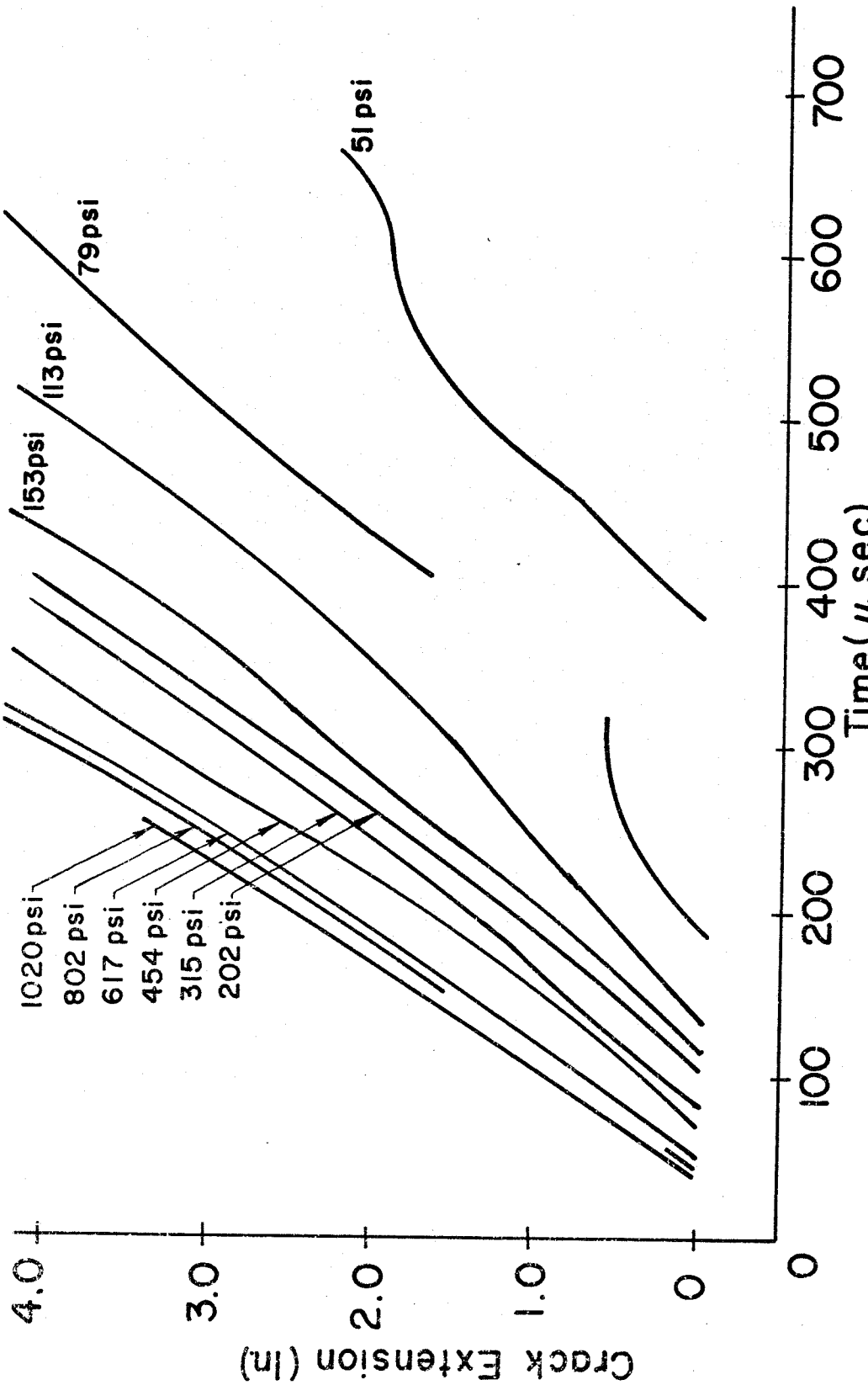

FIG. 26. Crack Extensions versus Time

Determination of the exact time at which initial crack growth occurred as well as the acceleration and velocity of the crack close to the initiation time are necessarily below the resolution inherent in the high speed photographic system. It is also true that regardless of the fineness of the resolution of the crack monitoring system, an uncertainty will exist as to the start and initial behavior of the crack. It was therefore necessary to devise a consistent criterion that can be used to characterize the onset of crack propagation. Near the time of crack initiation, the crack extension history exhibits a nearly linear relationship with time. Figure 27 shows the same data as Figure 26, but with an expanded ordinate scale and data points with error estimates included. The data are linearly extrapolated to intersect with the line of zero extension. The time corresponding to that intersection is chosen as the characteristic time of crack initiation. Experiments by Döll [55] on plexiglass indicated that a crack would accelerate from a few cm/s to $1.4\ 10^4$ cm/s in less than 0.10 mm. This would suggest that the criterion chosen could be quite reasonable. Table 2 summarizes the crack initiation times, the approximate crack terminal velocities, and the maximum value of the stress applied at the boundary, which occurred about 25 microseconds after the start of the experiments.

Figure 28 shows the stresses applied to the crack surfaces as a function of time for each of the experiments. These were determined by applying the calibration relation to the oscilloscope traces of the current. The time of fracture initiation is indicated on each curve. The correlation of the time to failure and the applied stress

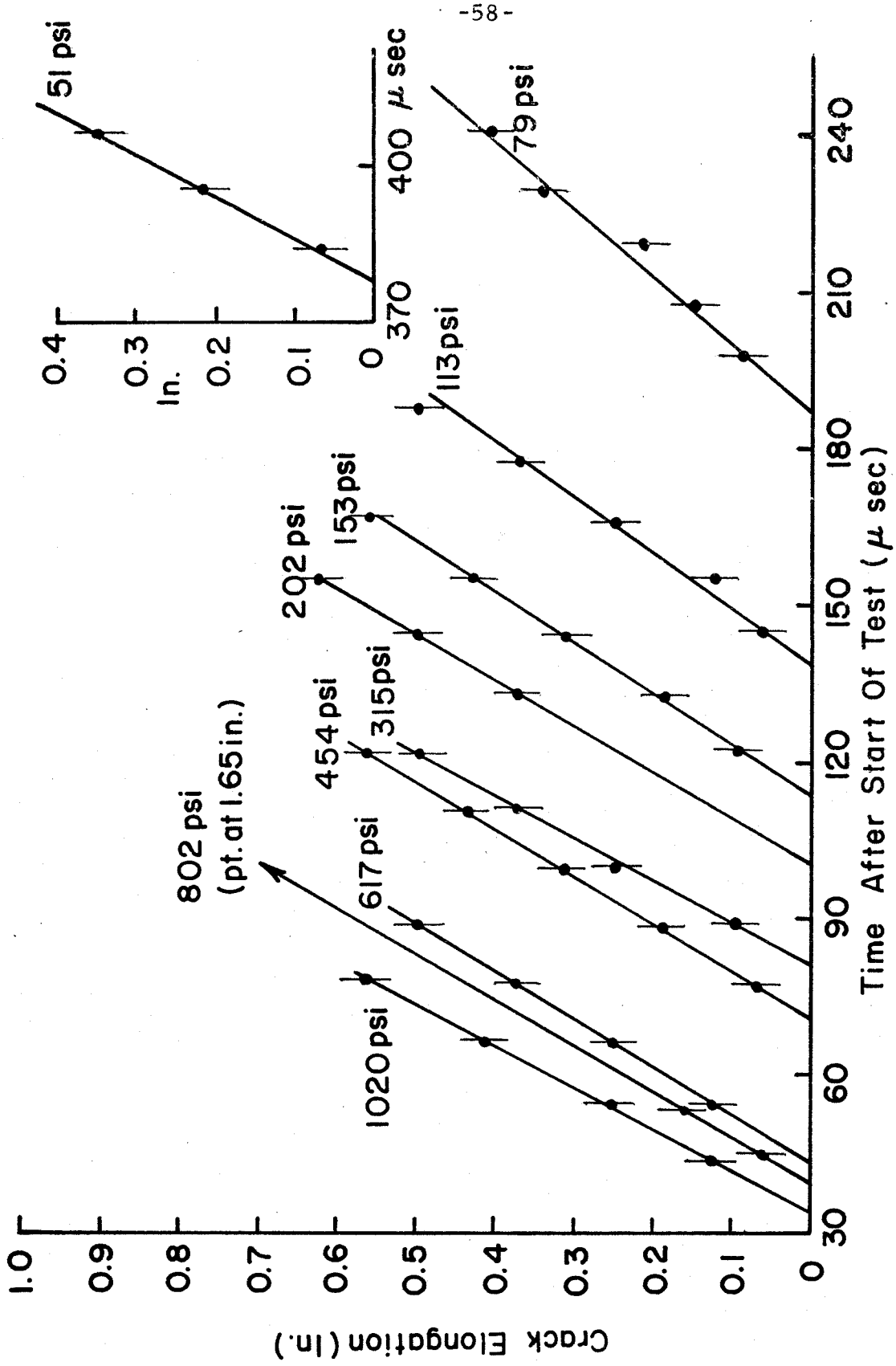

FIG. 27. Crack Extensions versus Time

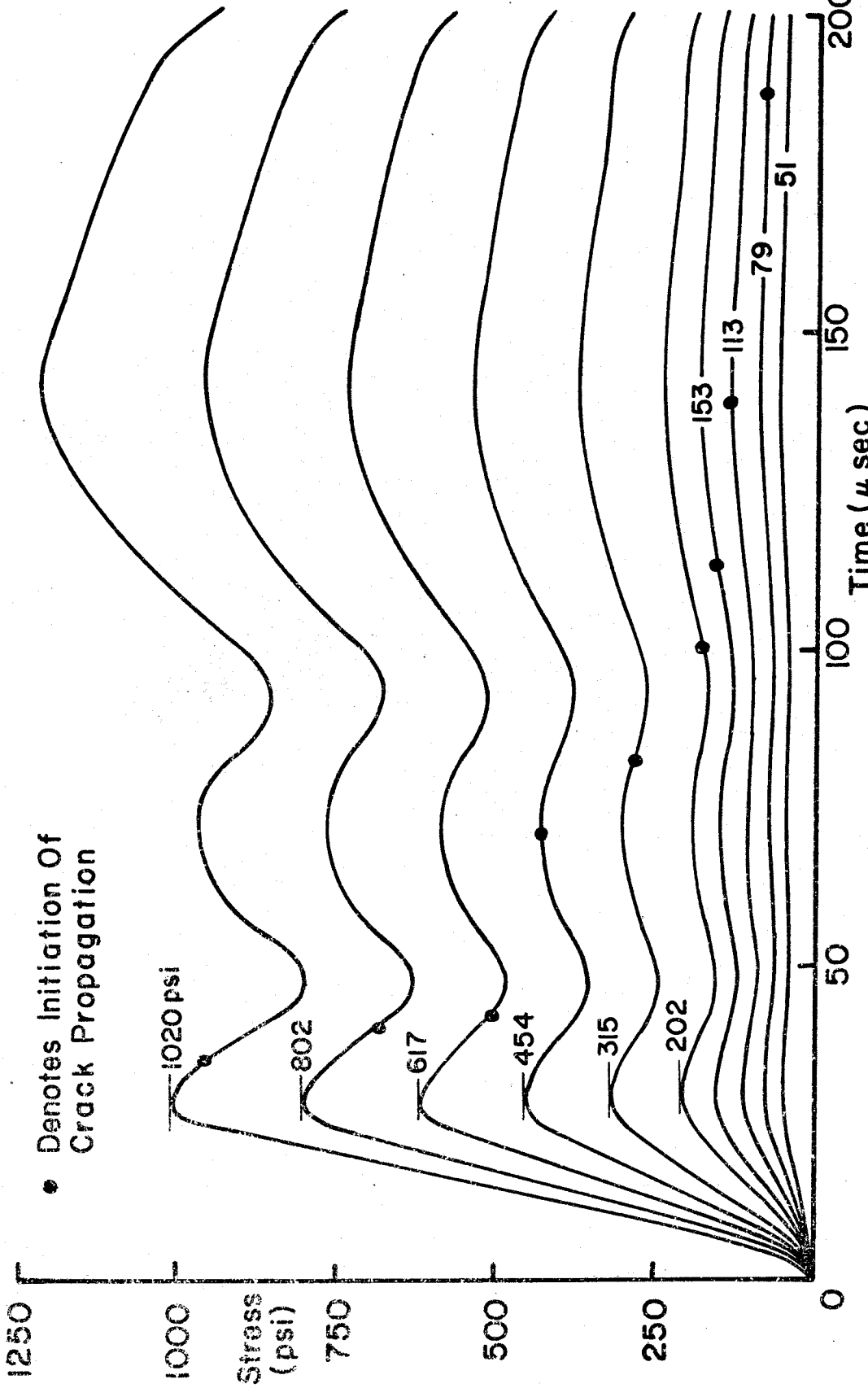

FIG. 28. Tractions Applied to the Crack Surfaces

Table 2

Boundary Traction after 25 μsec (psi)	Time for Crack Initiation (μsec)	Terminal Crack Velocity (in/sec)
51	399	-
79	187	10,600
113	139	12,500
153	113	14,500
202	100	15,000
315	81	16,000
454	71	17,500
617	43	17,500
802	40	17,500
1020	34	17,500

on the boundary would not, however, be expected to be highly significant since it is the stress state at the crack tip and not that along the crack surfaces which determines fracture. In the case of dynamic fracture, stress waves are generated on the crack faces and travel in the plate toward the crack tip at sonic speeds. Therefore, to characterize the fracture process, the stress state at the crack tip prior to and at the time of fracture had to be determined. The photographs of the photoelastic patterns about the crack tip did not show sufficient resolution for this purpose. As an alternative, an analysis was performed with the stress histories shown in Figure 28 as the applied boundary conditions. A description of the analysis and its results are presented in Chapter 7.

One peripheral result of the experiments had to do with crack branching during three tests at higher load levels. For the lower load levels the crack propagated along a nearly straight line colinear with the machined slot, and the surface generated by the propagating crack had a glassy smooth texture. The cracks that branched had the same behavior for approximately two inches of initial propagation. Beyond that the surface roughness increased progressively up to the branch point where extensive local material damage was evident. Prints made from the high speed camera negatives of different experiments are shown in Figure 29. The photographs indicate that in each case the crack formed three branches. One of the branches typically propagated along a line nearly colinear with the original propagating crack and the other two branches propagated along lines that were close to $\pm$ 45 degrees from the center branch. In the photograph of the experiment with the highest load, Figure 29c, it appears that one of the branches does not start simultaneously with the other two. Upon closer inspection of the failed specimen, it is observed that the region where branching initiated is highly damaged and the three branches started closer to one another than can be inferred from the photograph. For that same case, the center branch ran approximately 1" before it branched again into three crack segments. This time the outer branches propagated along lines that were approximately $\pm$ 22 degrees off the center branch. A summary of the branching data is listed in Table 3 below. After branching, each of the three new cracks had a velocity close to the 17,500 in/sec. For the highest load level, the two outer

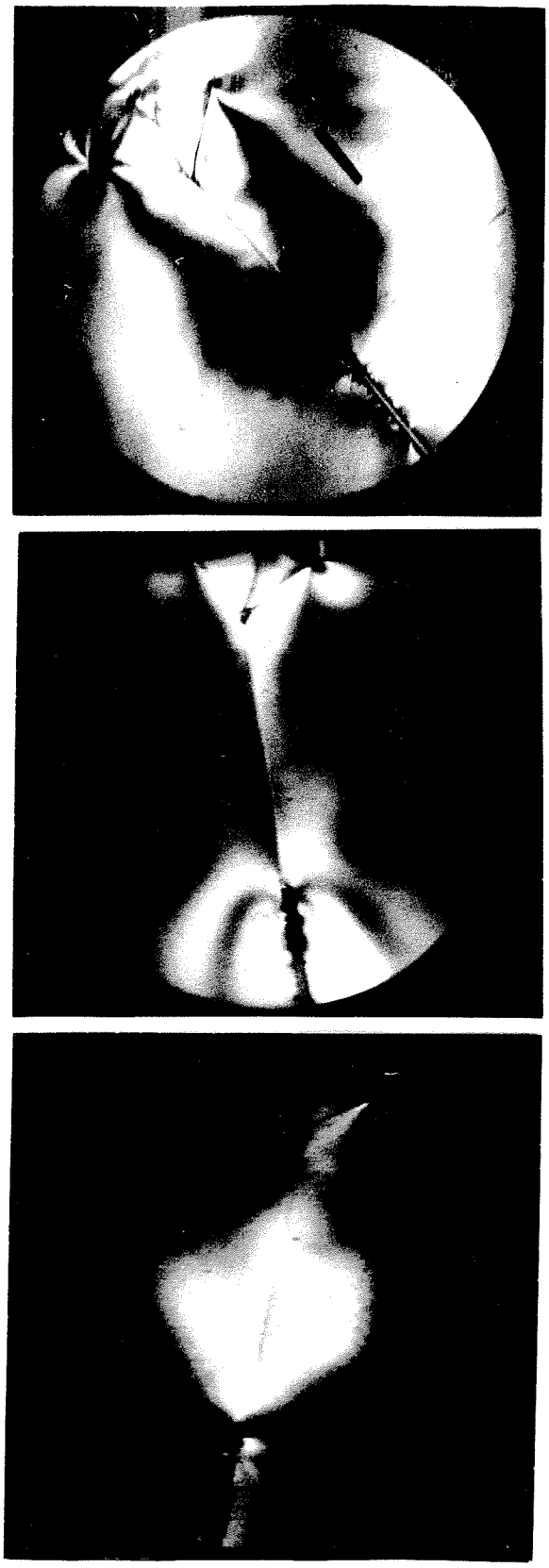

(a) (b) (c)

FIG. 29. Cinematographs Showing Crack Branching from Three Experiments

Table 3

Load Level (25 μsec after start of load) (psi)	Approximate Time at Branching (μsec)	Distance Traveled Before Branching (in)	Crack Velocity at Branching (in/sec)
617	344	4.1	17,500
802	333	4.1	17,500
1020	277	3.5	17,500

branches also branched again, but with only two branches. It is also of interest to note that the crack with the highest applied load branched before stress waves reflected from the edges of the plate had arrived at the region where branching occurred.

Branching had been observed previously in dynamic fracture experiments involving Homalite [4, 40]; however, the reported branching involved two branches. The difference between the experimental configuration used here and the previous dynamic fracture work that could account for the additional branch has to do with the nature of loading. In the previous work, the specimen was loaded statically until the crack ran which would develop a different stress field about the crack tip than that generated in this study by a dynamic loading device.

7. ANALYSIS OF EXPERIMENTAL DATA

The "modern" theory of fracture is founded on the proposition by Griffith [1] that the state of the material at the tip of a crack or flaw determines the fracture behavior of a solid. It follows then that the tractions applied at boundaries are significant in that they, as well as the specimen geometry and the material constitutive behavior, are elements that determine the material state near the crack tip. Griffith further proposed an energy balance criterion to describe the start of crack propagation, which incorporated the concept of an energy requirement for the creation of new surface. This criterion specifies that when the release rate, G, of strain energy by the extension of a crack exceeded the rate of energy necessary for the creation of new surfaces, γ, fracture could occur; i.e., a crack becomes unstable when

$$G = 2\gamma \tag{5}$$

Experimental evidence by Griffith and others [56] tend to support the energy balance criterion. A measure of the strain energy release rate is required for the application of the criterion and is generally obtained from a linear elastic solution for the stress state in the solid. The analyses typically involve a two-dimensional model of what is called an "ideal" crack, represented by a straight line discontinuity in the solid. Near an end of an ideal crack, which has zero radius of curvature, a singular stress field exists. The coefficient of the singularity, as mentioned earlier, is called the stress intensity factor K. For the case of symmetric loading, which

involves only a crack opening mode, Irwin has shown that the stress intensity factor can be expressed in terms of the strain energy release rate [2]. Since it is necessary to determine K in order to calculate G, the common practice now is to consider only K in discussions of fracture. The above comments have dealt with static loading cases; however, the basic concept carries over to the dynamic case. The analysis, of course, is complicated by the inclusion of the inertia terms in the governing equations and the addition of a kinetic energy term in the energy balance criterion. The relation between the dynamic stress intensity factor, which is a function of time, and the strain energy release rate, has the form

$$G = \frac{1-\nu^2}{E} K^2 A(\dot{\ell}) \tag{6}$$

where E and ν are Young's modulus and Poisson's ratio respectively and $A(\dot{\ell})$ is a crack velocity dependent factor [17]. For a stationary crack, $A(\dot{\ell})$ is identically equal to unity.

Thus, if the energy criterion used to predict the start of a crack propagation for the static case is valid for the dynamic case, then there would be a corresponding critical stress intensity factor that could be used to describe the onset of crack propagation. That question is addressed in the remainder of this chapter. First, however, it is necessary to discuss the analysis used here to calculate the stress intensity factor.

Freund [18] has given the solution to the plane strain problem of a semi-infinite crack in an unbounded elastic solid that suddenly has equal but opposite concentrated forces applied on the

crack surfaces. (See Figure 30 below.)

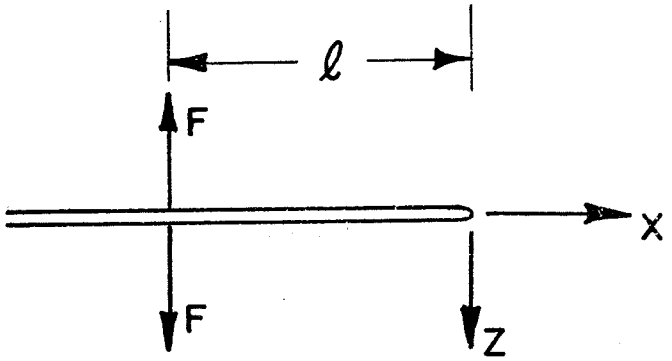

FIG. 30

The problem was solved by substituting displacement potentials into the governing equations. Application of a Laplace transform on time and a bilateral Laplace transform on the spatial variable x, followed by the elimination of the parameters of integration, yield a single Wiener-Hopf type equation. This equation was factored and the unknown normal stress, σ_{zz}, along the line $z = 0$ and for $x > 0$ was then determined directly. The time dependent stress intensity factor was then found from the following limit

$$K(t;\ell) \equiv \lim_{x \to 0^+} (2\pi x)^{\frac{1}{2}} \sigma_{zz}(x, 0, t;\ell) \tag{7}$$

The solution for the problem of sudden concentrated equal and opposite forces on crack faces forms a Green's function that can be used for any general spatial and time-varying loading by the superposition

$$K'(t) = \int_0^t ds \int_0^\infty K(s;\ell)p(\ell)\, \dot{f}(s)\, d\ell \tag{8}$$

where $p(\ell)$ is the spatial pressure distribution function and $\dot{f}(s)$ is the derivative of the time-dependent proportionality factor for the

applied tractions. A computer program was written to integrate Eqn. (8) numerically; $p(\ell)$ and $\dot{f}(s)$ are arbitrary and determined in the experiments by the particular experimental circumstances. A minor deviation from Freund's plain strain solution was incorporated with respect to dilatational wave propagation. Instead of plane strain conditions, the experimental arrangement resembles a plane stress condition as the plate thickness, 3/16", is small, as discussed in Chapter 3, relative to the wavelength of 8" for a wave with a quarter period equal to the risetime of the stress pulse applied to the crack faces. Since the plate and loading conditions closely resembled the plane stress condition, the usual adjustment was made of substituting the plate velocity for the dilatational velocity [58].

The computer program was checked by solving particular problems and comparing the results with known closed form solutions. A discussion of two of these problems is instructive with regard to the experimental effort and is therefore presented here.

The first of these is the problem (discussed in Chapter 2) of a sudden pressure applied uniformly along the faces of a semi-infinite crack. The following table lists the normalized stress intensity factor determined from Baker's [14] solution for the normalized stress intensity factor and that from the computer program under similar conditions. The difference between the two values of stress intensity factors for this example, which is small, results from the fact that some arbitrary small distance close to the crack tip remains unloaded for the computer solution. This poses no

Table 4

Time (μsec)	K_I (Baker)	K_I (Green's Function)
0	0	0
20	1.346	1.289
40	1.903	1.857
60	2.331	2.306
80	2.691	2.666
100	3.009	2.983
120	3.296	3.264
140	3.560	3.492

difficulty for the analysis of the experimental work since the short hairline extension of the machined slot in the specimen was not loaded either. In fact, the capability of accounting for an arbitrary unloaded length near the crack tip was the motivation for using this Green's function solution.

Another check of the computer program involves the comparison of a known static stress intensity with the dynamic stress intensity factor after a sufficiently long time. Long time in this case refers to the time required for the passage of the slowest wave that would have an influence on the material near the crack tip. Consider for example the tractions shown in Figure 31.

If the tractions were not a function of time (i.e., the static case), then the stress intensity factor could be found from Eqn. (9).

$$K_I = \sqrt{\frac{2}{\pi}} \int_{-\infty}^{0} \frac{p(x)dx}{\sqrt{-x}} \qquad (9)$$

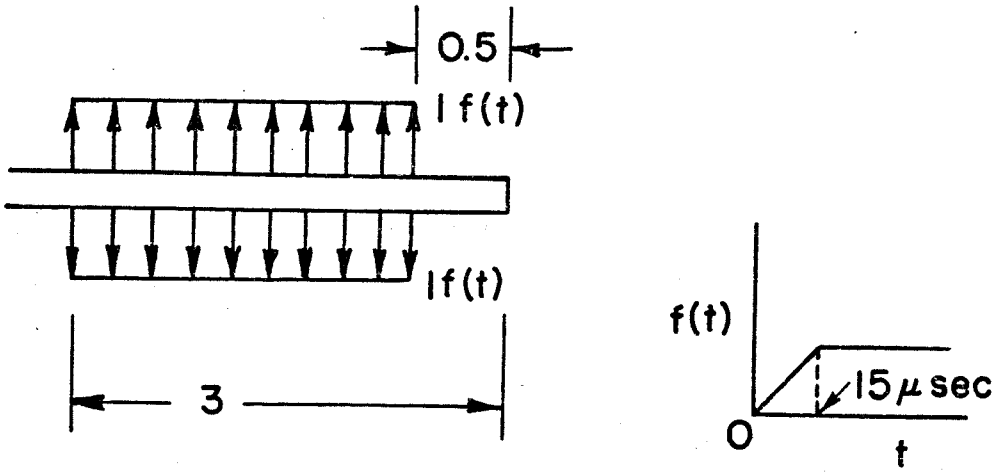

FIG. 31

The spatial distribution as shown in Figure 31 is

$$p(x) = 1\ H(x - \tfrac{1}{2})H(3-x) \qquad (10)$$

where H is the Heaviside step function. Solution of Eqn. (9) with p(x) given by Eqn. (10) yields a stress intensity factor of 1.635.

For the case where the tractions are the function of time shown in Figure 31, which is an arbitrary example, the dynamic stress intensity factor found with the computer program is shown in Figure 32.

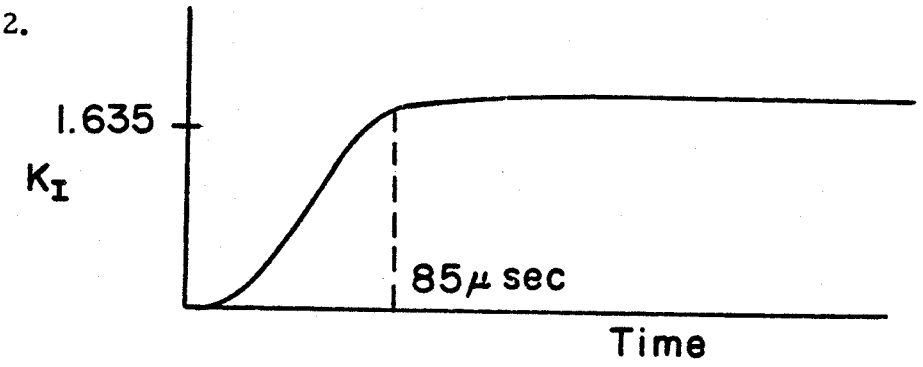

FIG. 32

Dynamic Stress Intensity Factor for the Example Shown in Fig. 31

The time of 85 microseconds equals, as expected, the loading rise-time plus the time required for a disturbance travelling at the Rayleigh speed (slowest wave velocity in the solid) to travel the 3" to the crack tip in a material possessing the elastic properties of Homalite.

From this later problem it can be seen that the Rayleigh wave, which can be described as a phenomenon associated with a free surface, is significant with respect to the physics of the problem. The fact that a thin copper strip is bonded to the crack faces would necessarily affect the Rayleigh wave behavior. Also, the three-dimensional aspect of the problem along the corners formed by the crack faces and the sides of the plate would also tend to alter the Rayleigh wave behavior.

Despite these departures from what might be considered ideal boundary conditions, it remains true that a highly repeatable family of normal tractions can be applied to the faces of the crack. Since the copper strip is quite thin (0.02") compared to characteristic wavelengths (8"), behaves as an elastic solid, and has one free surface and the other bonded to the specimen, the approximation of a crack in homogeneous material would appear reasonable.

The computer program was found useful in assessing the sensitivity of the stress intensity factor to small changes in loading parameters. Two parameters, in particular, were considered candidates for investigation. The first of these had to do with the risetime associated with the boundary tractions. The stress intensity factor was previously known for the case of the step

function in time. For the purpose of comparison, the stress intensity factors were calculated for the cases of ramp loading to a constant value. The durations of the ramps were chosen as 20 and 50 microseconds. In all three of the examples, the tractions were applied uniformly along the crack surfaces starting at the crack tip. The results of this investigation are shown in Figure 33. The conclusion is that the rate of loading is a significant parameter in calculating the dynamic stress intensity factor, but the low variability of risetimes (less than a microsecond) that can be achieved with the electro-mechanical loading approach results in a stress intensity factor that is rather insensitive to risetime variations between the tests reported here.

The second parameter that was investigated for effect of variability on the stress intensity factor was the distance of the stress-free boundary between the crack tip and the loaded portion of the crack surface. The computer program was used to calculate the dynamic stress intensity factor for the cases of a load being applied as a step in time and for stress-free lengths of 0.2" and 0.5" from the crack tip. The results of this study are shown in Figure 34. The conclusion which can be drawn from this figure is similar to that drawn from the study of variation in time; namely, the effect is significant but is relatively insensitive to small variations in the length of stress-free regions. The stress-free regions for the experiments varied from 0.125" to 0.1875".

The ultimate objective in developing the general program was to compute the dynamic stress intensity factor as a function of

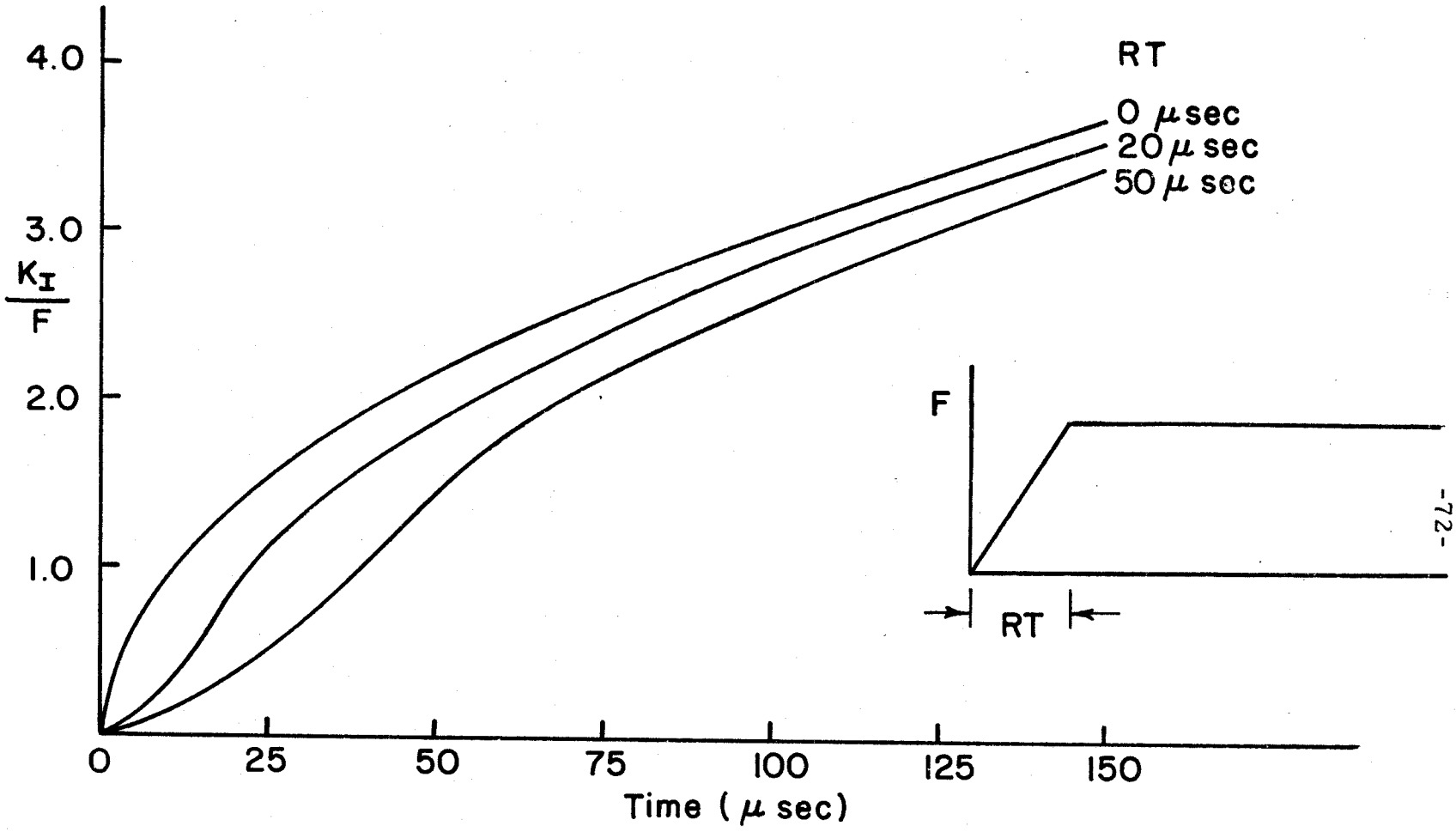

FIG. 33. Stress Intensity Factor Versus Time

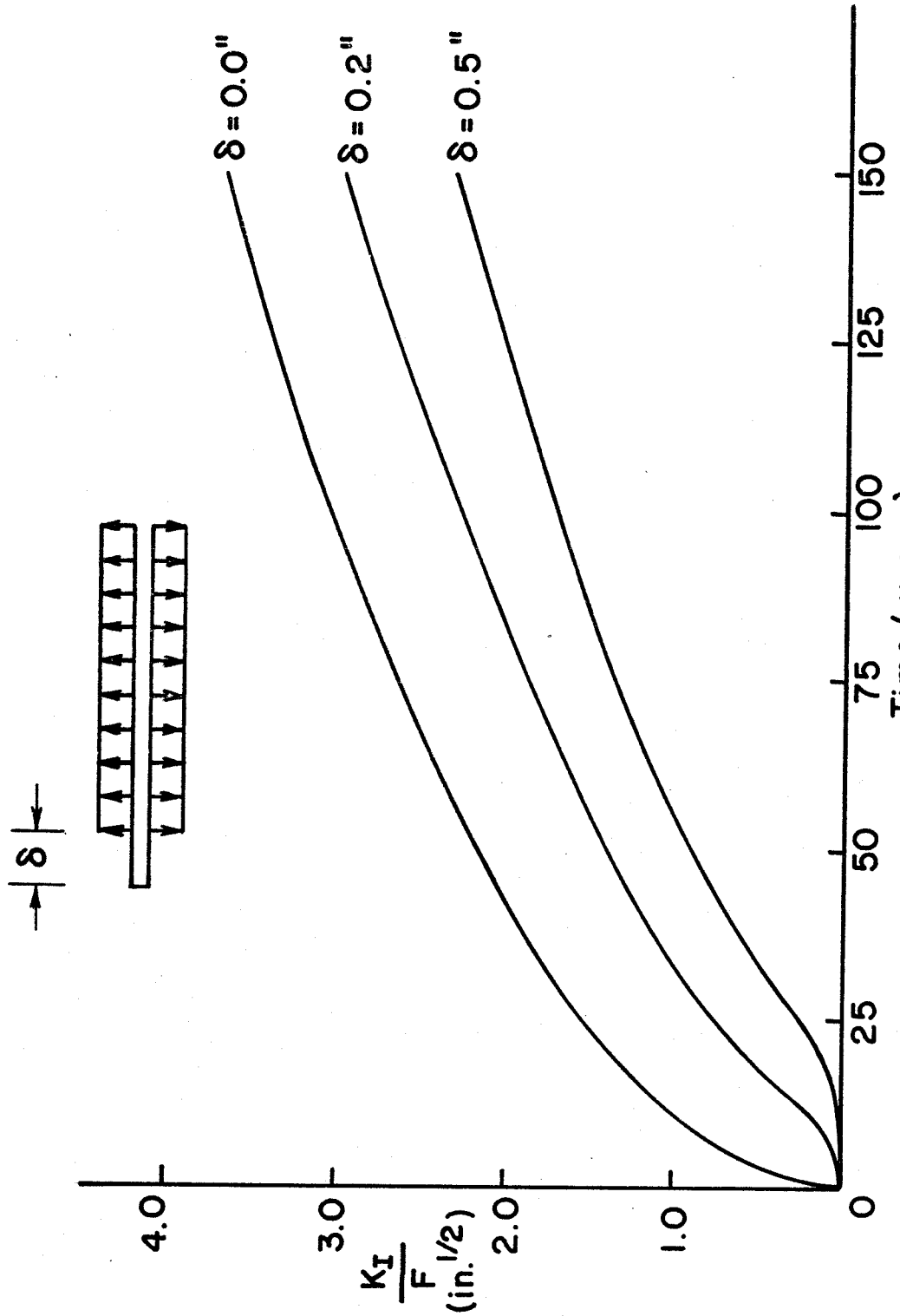

FIG. 34. Stress Intensity Versus Time

time for each load history recorded experimentally. It was found that the load histories that could be measured from an oscilloscope were indistinguishable except for a scale factor relating to the load level. Since the unloaded region near the crack tip varied only slightly, the dynamic stress intensity factor was found for a particular case and scaled according to the stress level.

In order to use the Green's function approach, it is necessary to specify a spatial representation of the applied stress along the crack surfaces and a time history of that stress. A representation of these distributions is shown in Figure 35 and they are discussed below.

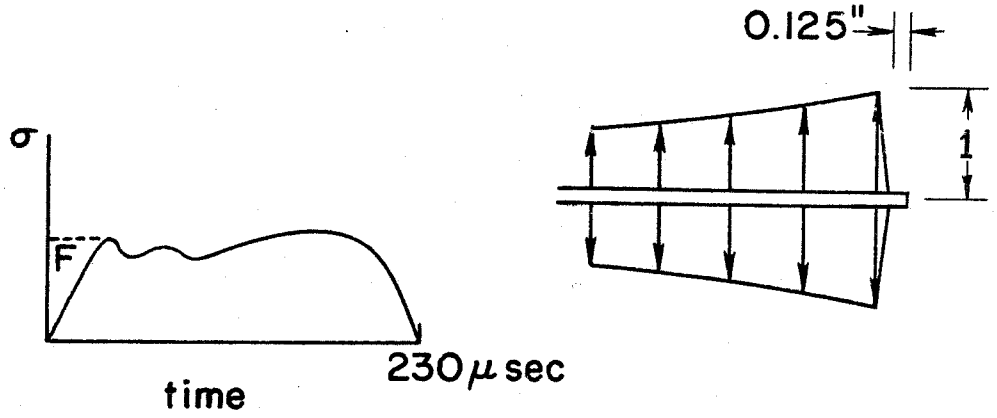

FIG. 35

Schematic of Time History and Modified Spatial Distribution Used in Calculation of Experimental Stress Intensity Factors

The time history of the applied loading was calculated from the current trace recorded during each experiment (shown in Figure 28). The spatial distribution of the tractions applied to the crack surface was identically zero from the crack tip to the outside radius of the copper loading strip. It was assumed that the stress increased

linearly from the outside radius of the copper strip to the inside radius (a distance of 0.02"). From the inside radius of the strip to the edge approximately 18" away, the applied loading was taken as unity. From the strain gage calibration of the loading device (discussed in Chapter 5), it was known that attenuation of stress waves in Homalite occurs as the wave propagates. This attenuation was compensated for by modifying the spatial distribution of the applied tractions. The modification was accomplished by multiplying the spatial distribution by an exponential that decayed along the crack faces with increasing distance from the crack tip. The rate of decay was taken to be identical to that found in the attenuation measurement during calibration (shown in Figure 22). The distributions shown in Figure 31 depart from the "ideal" case that was originally sought and which is shown in Figure 36 below. The

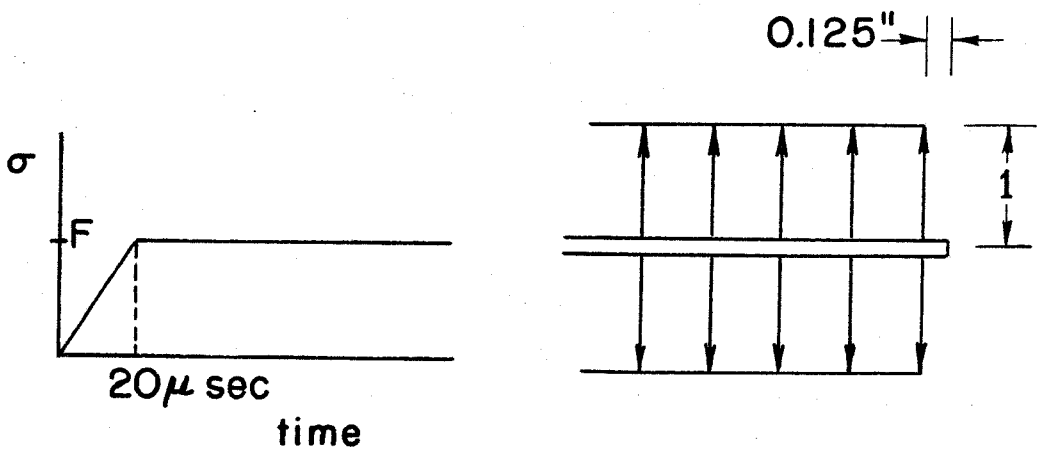

FIG. 36

Schematic of an Ideal Time History and Spatial Distribution

stress intensity factors for the actual case shown schematically in Figure 35 and the ideal case shown in Figure 36 were calculated with the computer program and are shown in Figure 37. It can be seen from the figure that, although the boundary conditions between the cases are significant, the stress intensity factors for the two cases are quite similar. The stress intensity factor that was determined from the experimental data has a maximum at about 200 microseconds which corresponds to the time at which the level of the applied loads begins to decrease. Until that maximum, the stress intensity factor approximately increases linearly with time. That approximation will be useful in a subsequent discussion of a simple model of the fracture behavior.

The dynamic stress intensity factors, calculated using experimental data, are shown for the ten fracture experiments in Figure 38. The points on the curves indicate the onset of crack propagation and were determined from the high speed photographs, as described in Chapter 6. It should be noted that the Green's function solution for the stress intensity factor is only valid until the instant the crack begins to propagate. Freund [17] gives a solution for the stress intensity factor when the crack is moving, but that information is not needed for this analysis.

The value of the stress intensity factor (discussed above) when the crack becomes unstable and propagates rapidly is called the critical stress intensity factor or the (dynamic) fracture toughness, which is generally taken as an intrinsic material property. It will be recalled that a principal objective of this study was to determine

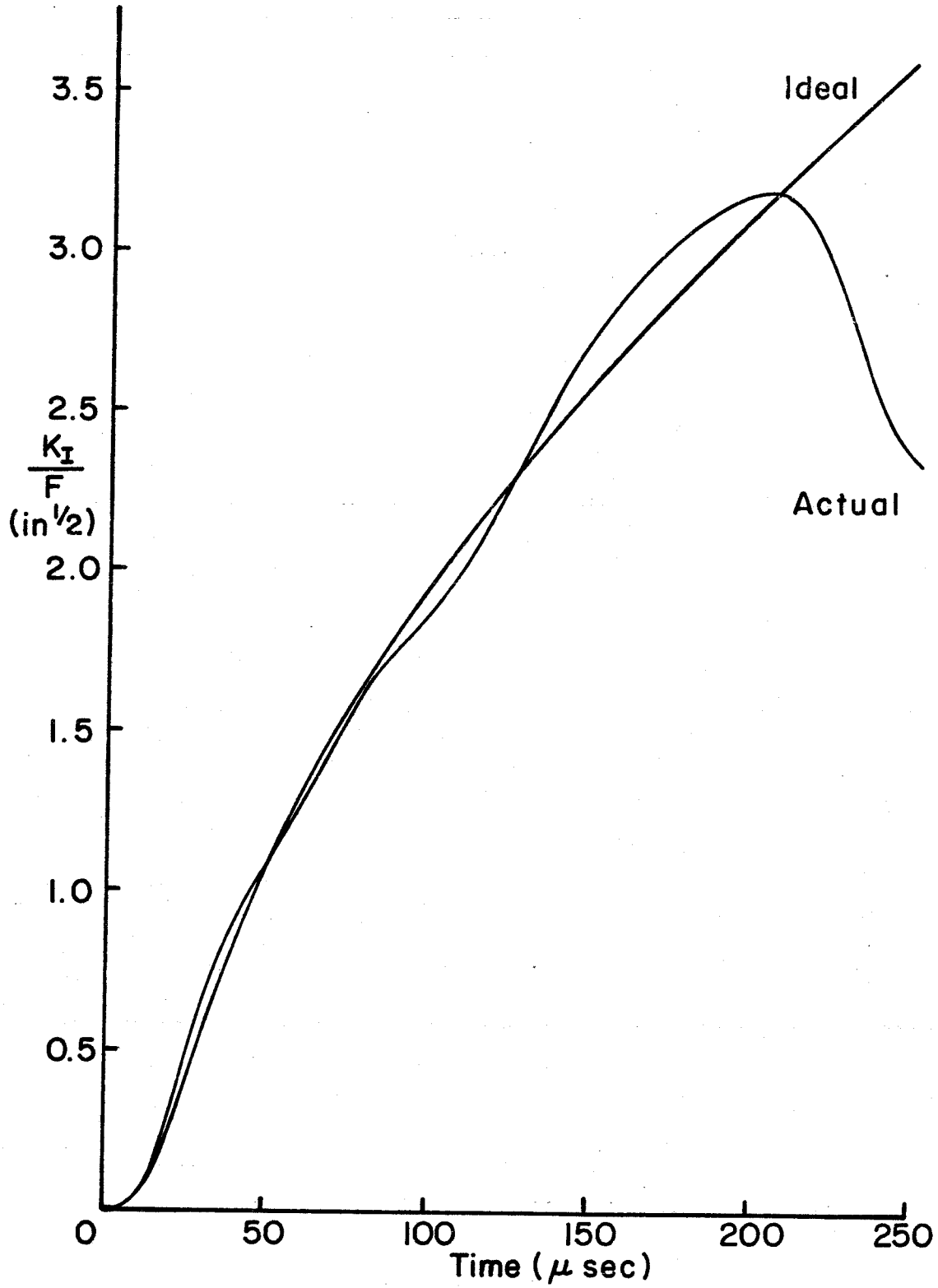

FIG. 37. Normalized Stress Intensity Factor versus Time

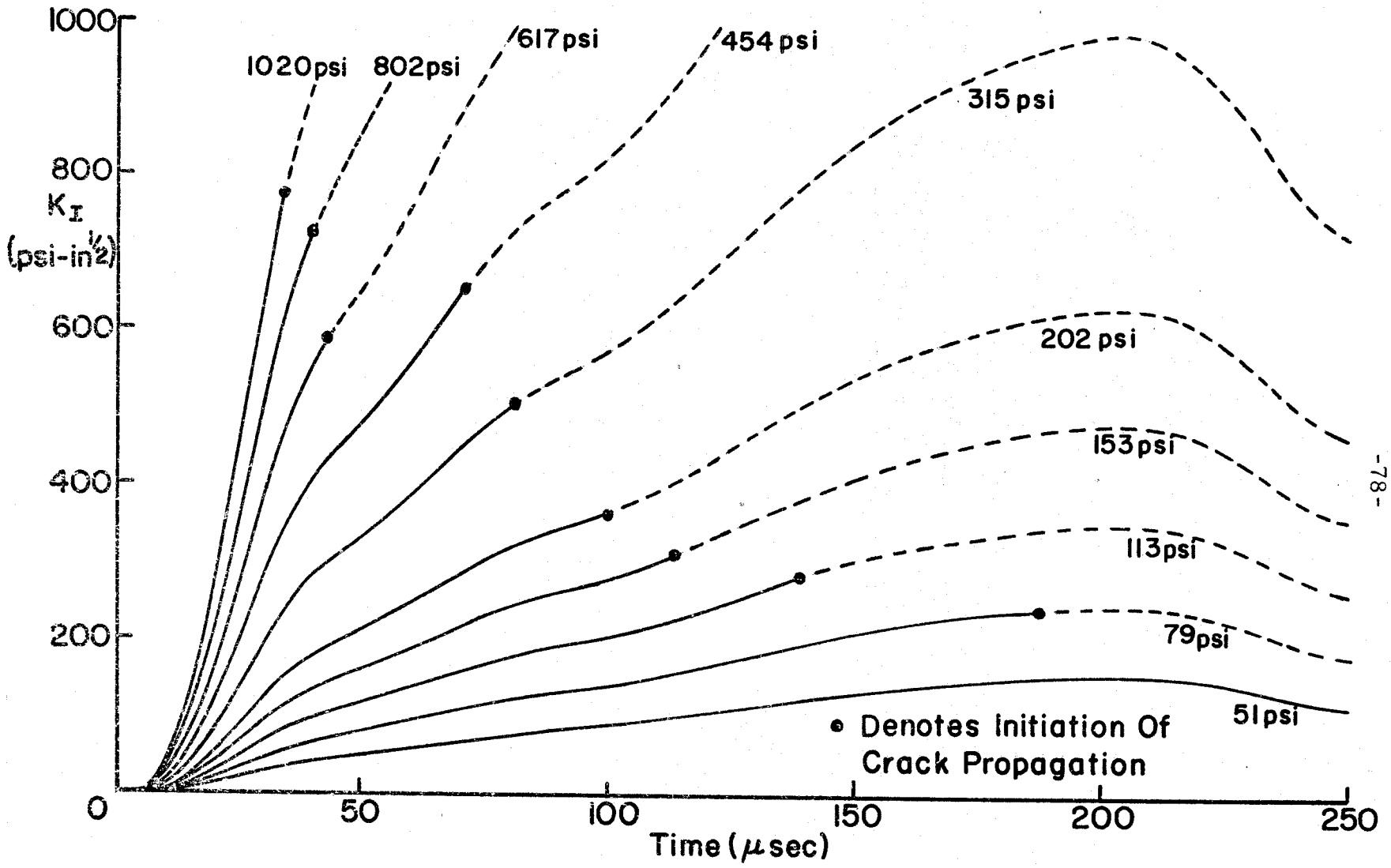

FIG. 38. Stress Intensity Factors versus Time

the effect of loading rate on the critical stress intensity factor. To accomplish this, several standard fracture toughness tests were performed on compact tension specimens at low loading rates with an Instron test machine. Bradley [6] performed a series of similar fracture toughness tests at a single rate* which was lower than that which could be achieved with the Instron. The fracture toughness for these quasi-static tests, as well as the data from the dynamic tests, are plotted in Figure 39, against the logarithm of the time to failure. For the quasi-static tests, the rate of loading was linear with time. For the dynamic tests, the rates correspond to the slopes of the curves in Figure 38.

The data of Figure 39 seem to indicate the existence of a minimum value of the fracture toughness. (For convenience, it will be referred to as the "minimum" in subsequent discussions.) A possible explanation of the observed behavior of the fracture toughness has to do with the viscoelastic behavior of the material. Of course, the material at the crack tip is highly strained and a precise description of the constitutive behavior at such strains is unknown.** It would not be unreasonable though to expect significant plastic or viscoelastic deformation to occur close to the crack tip where the strain gradients are, due to the sharpness of the crack tip and the

---

*Inferred from Bradley's description of specimen and crosshead speeds.

**In fact, the reason for performing tests with cracked specimens is that it is the only reasonable method known of achieving the constitutive state at the crack tip.

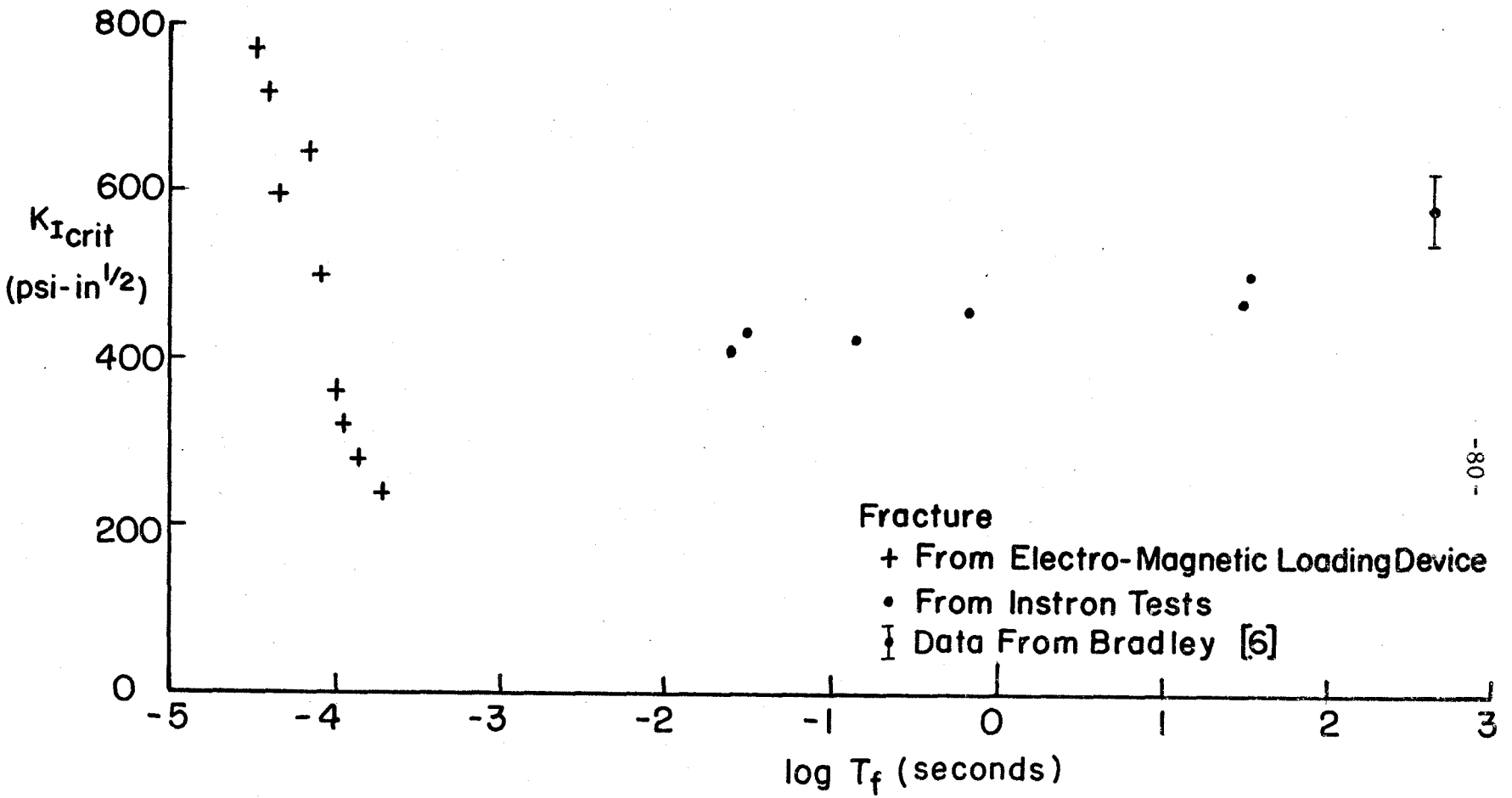

FIG. 39. Fracture Toughness Versus Time to Failure

resulting stress concentration, quite large.

If one postulates viscoelastic behavior in a region close to the crack tip for rates sufficiently slow (i.e., quasi-static) then the relaxation associated with creep would tend to unload the crack tip. This would mean that fracture events with longer times to failure would have longer times for the material to relax near the crack tip and in effect could withstand higher applied loads. Since stress intensity factors are calculated on the basis of linear elasticity, the critical stress intensity factor would be higher for such cases.

The above discussion pertained to rates of loading that were quasi-static. The data in Figure 39 clearly indicate that at very high loading rates the fracture toughness is highly dependent on the rate of loading, but in that case, it increases with increasing rate. This fact suggests that some factor that was not significant for quasi-static loading becomes dominant for dynamic loading. It is known that for dynamic crack propagation the temperature at the crack tip rises to quite high values. For the organic glass PMMA, this mean temperature rise was calculated to be about 400°K, using measurements of the infrared radiation from the crack tip by Fox and Fuller [72] and Fuller, Fox and Field [73]. Weichert and Schönert [69] have also found temperature rises on the order of 1000°K for glass and steel using light emission measurement techniques.

Although the temperature rises discussed above pertain to running cracks, it is not unreasonable to expect some similar

effects to occur for the high loading rates that can be achieved with the electromagnetic loading device. Increasing the temperature of a viscoelastic material shifts the relaxation spectrum to shorter times (i.e., the material becomes more viscous). Hence the abrupt increase in toughness for the very fast loading rates may also be due to relaxation, in the highly local region surrounding the crack tip, which is a result of the strongly non-linear interaction of temperature and material behavior.

Let us now consider a very simple idea on how the result of fracture may be related to the time history of the stress intensity factor. It is based on ideas that have been used to explain the apparent increase in toughness of metals observed in spallation experiments by Field [66]. The model is an extension of one devised by Dugdale [67] to account for plasticity at a crack tip and by Barenblatt [68] to circumvent the singular stress, at the crack tip, that is found from elastic analyses. Dugdale assumed that there exists a yielded zone extending from the crack tip as shown in Figure 40 where δ is the crack tip opening displacement. For a

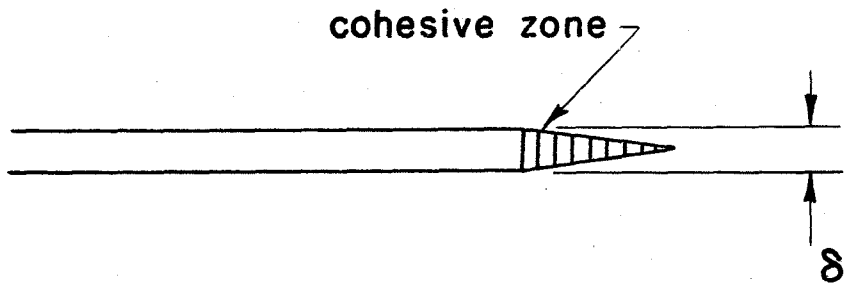

FIG. 40

Dugdale-Barenblatt Model

uniform stress, σ_o, in the cohesive zone, the crack opening displacement can be represented in terms of the stress intensity factor, K_I, and the material properties outside of the zone by the following expression

$$\delta = \frac{\kappa+1}{8G} \frac{K_I^2}{\sigma_o} \tag{11}$$

where G is the shear modulus and, for plane strain, $\kappa = 3-4\nu$ [70]. Goodier and Field [71] assumed that fracture for a material having such a cohesive zone occurred when the strain at the crack tip reached a critical value, ϵ_u, defined by

$$\epsilon_u = \delta/\ell \tag{12}$$

where ℓ is the initial unstrained length. Field [66] extended this model for dynamic loading situations by stipulating that the stress resisting the opening of the elastic region (i.e., σ_o) is time dependent and governed by an appropriate rate law.

For the present purpose, let us try to describe the high rate fracture observed here by assuming that σ_o is proportional to the strain rate. This assumption is roughly consistent with the previous argument that heating causes the crack tip region to be highly viscous. Since the rate of loading was nearly linear in the experiments, it was convenient to characterize the strain rate by

$$\dot{\epsilon} = \frac{\epsilon_u}{\tau} \tag{13}$$

where τ is the time at failure and ϵ_u is the strain at failure and,

following Goodier and Field, is assumed to be a constant.* Combining Eqns. 11, 12 and 13, one finds that the stress intensity factor at failure (i.e., the fracture toughness) is given by

$$K_I = \frac{\text{constant}}{\tau^{\frac{1}{2}}} \tag{14}$$

The primary data from the high rate fracture experiments were the values of K_I and τ at failure. These points are plotted in Figure 41. Also shown in the figure are Eqn. 14 and a curve representing a least square exponential fit of the experimental data.

While the model is very crude and its evaluation correlates only with a limited portion of the experimental results, its simplicity allows consideration of the basic aspects of a very complex process. The similar slopes of the two curves plotted in Figure 41 suggest that the hypothesis of local heating causing increased viscous effects may be valid. The apparent heating effect at high loading rates on the fracture toughness found here may also extend to other classes of materials. The loading device built for this work could be effectively used to study that question further.

---

*This constant is unknown and the theoretical results accordingly can only be found to within a constant.

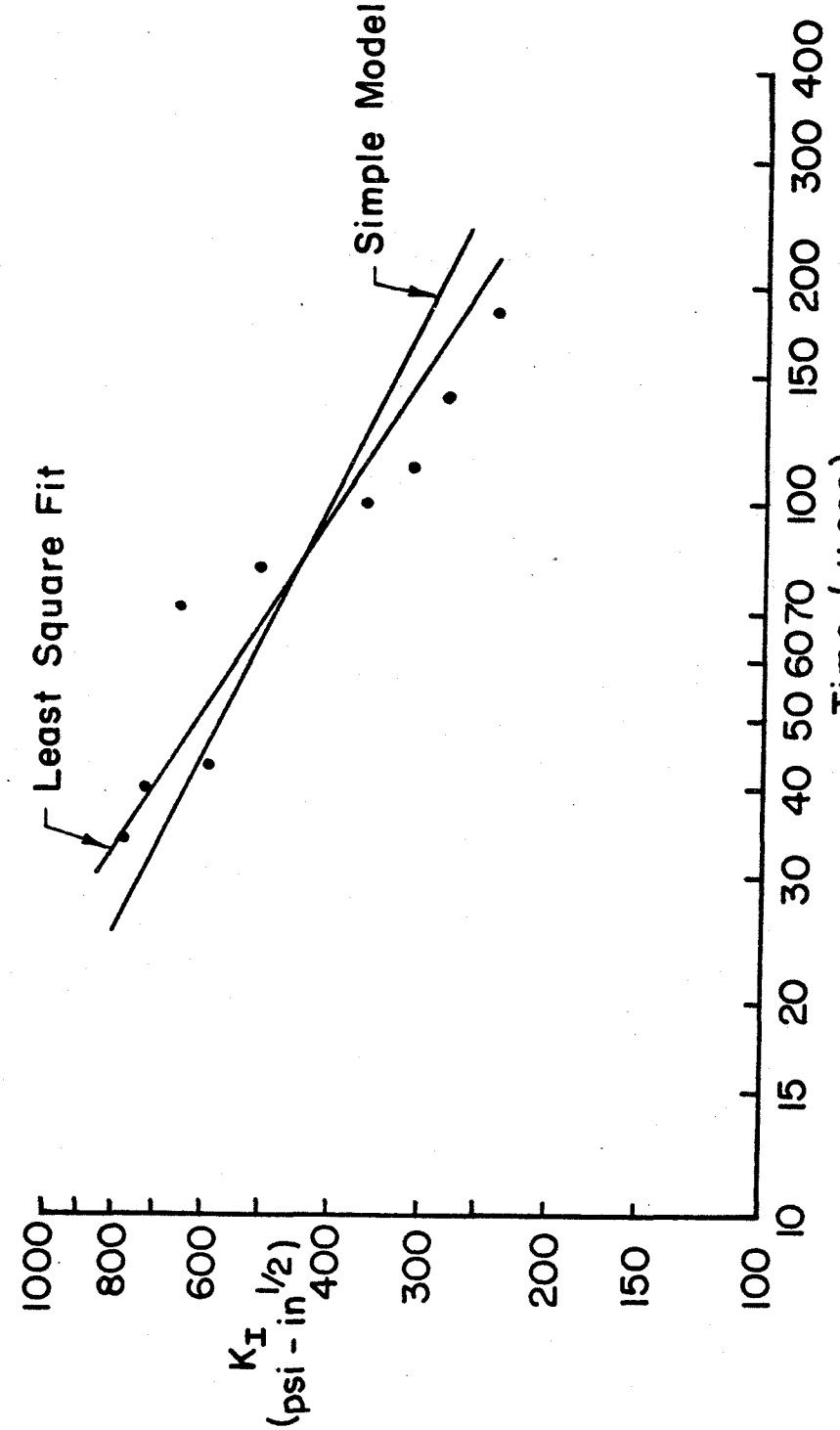

FIG. 41. Fracture Toughness Versus Time to Failure

REFERENCES

1. Griffith, A. A., "The Phenomena of Rupture and Flow in Solids," Philosophical Transactions of the Royal Society, London: Series A, Vol. 221, 1920, pp. 163-198.

2. Irwin, G. R., "Fracture," Handbuch der Physics, Vol. VI, edited by S. Flügge, Berlin: Springer-Verlag, 1958, pp. 551-590.

3. Kolsky, H. and Rader, D., "Stress Waves and Fracture," Fracture, Vol. I, edited by H. Liebowitz, New York: Academic Press, 1968, pp. 553-571.

4. Bradley, W. D. and Kobayashi, A. S., "Fracture Dynamics - A Photoelastic Investigation," Engineering Fracture Mechanics, Vol. 3, 1971, pp. 317-332.

5. Erdogan, F., "Crack-Propagation Theories." Fracture, Vol. II, edited by H. Liebowitz, New York: Academic Press, 1968, p. 559.

6. Bradley, W., "A Photoelastic Investigation of Dynamic Brittle Fracture," Ph. D. Thesis, University of Washington, Seattle, 1969.

7. Steverding, B. and Lehnigk, S. H., "Response of Cracks of Impact," Journal of Applied Physics, Vol. 41, 1970, pp. 2096-2099.

8. Steverding, B. and Lehnigk, S. H., "Dynamics of Brittle Fracture," International Journal of Fracture Mechanics, Vol. 8, 1972, pp. 59-73.

9. Steverding, B. and Lehnigk, S. H., "Impact and Fracture," Ceramic Bulletin, Vol. 49, 1970, pp. 1057-1061.

10. Yoffe, E. H., "The Moving Griffith Crack," Philosophic Magazine, Vol. 42, 1951, pp. 739-750.

11. Sih, G. C., "Some Elastodynamic Problems of Cracks," International Journal Fracture Mechanics, Vol. 4, 1968, pp. 51-67.

12. Maue, A. W., Die Entspannungswelle bei plötzlichem Einschnitt eines gesannten elastischen Körpers, Z. Angew. Math. Mech., Vol. 34, 1954, pp. 1-12.

REFERENCES (Cont'd)

13. Ang, D. D., "Some Radiation Problems in Elastodynamics," Dissertation, California Institute of Technology, Pasadena, California, 1958.

14. Baker, B. R., "Dynamic Stresses Created by a Moving Crack," Journal of Applied Mechanics, Vol. 32, 1962, pp. 449-459.

15. Achenbach, J. D. and Nuismer, R., "Fracture Generated by a Dilatational Wave," International Journal of Fracture Mechanics, Vol. 7, 1971, pp. 77-88.

16. Atkinson, C. and Eshelby, J. D., "The Flow of Energy into the Tip of a Moving Crack," International Journal of Fracture Mechanics, Vol. 4, 1968, pp. 3-8.

17. Freund, L. B., "Crack Propagation in an Elastic Solid Subjected to General Loading - II. Non-Uniform Rate of Extension," Journal of the Mechanics and Physics of Solids, Vol. 20, 1972, pp. 141-152.

18. Freund, L. B., "The Stress Intensity Factor Due to Normal Impact Loading on the Faces of a Crack," International Journal of Engineering Science, Vol. 12, 1974, pp. 179-189.

19. Achenbach, J. D., "Extension of a Crack by a Shear Wave," Zeitschrift für Angewandte Mathematik und Mechanik, 1970, pp. 887-900.

20. Sih, G. C., Embley, G. T. and Ravera, R. S., "Impact Response of a Finite Crack in Plane Extension," International Journal of Solids and Structures, Vol. 8, 1972, pp. 977-993.

21. Thau, S. A. and Lu, T., "Transient Stress Intensity Factors for a Finite Crack in an Elastic Solid Caused by a Dilatational Wave." International Journal of Solids and Structures, Vol. 7, 1970, pp. 731-750.

22. Freund, L. B., "Crack Propagation in an Elastic Solid Subjected to General Loading - I. Constant Rate of Extension," Journal of Mechanics and Physics of Solids, Vol. 20, 1972, pp. 129-140.

23. Freund, L. B., "Crack Propagation in an Elastic Solid Subjected to General Loading - III. Stress Wave Loading," Journal of the Mechanics and Physics of Solids, Vol. 21, 1973, pp. 47-61.

REFERENCES (Cont'd)

24. Freund, L. B., "Crack Propagation in an Elastic Solid Subjected to General Loading - IV. Obliquely Incident Stress Pulse," Journal of the Mechanics and Physics of Solids, Vol. 22, 1974, pp. 137-149.

25. Freund, L. B. and Rice, J. R., "On the Determination of Elastodynamic Crack Tip Stress Fields," International Journal of Solids and Structures, Vol. 10, 1974, pp. 411-417.

26. Hopkinson, J., Collected Scientific Papers, Vol. ii, 1872, p. 316.

27. Hopkinson, B., "The Effects of Momentary Stresses in Metals," Proceedings of the Royal Society, London: Series A, Vol. 74, 1905, p. 498.

28. Hopkinson, B., Collected Scientific Papers, Cambridge: University Press, 1921, p. 423.

29. Kolsky, H. and Shearman, A. C., "Investigations of Fractures Produced by Transient Stress Waves," Research, Vol. 2, 1949, p. 384.

30. Kolsky, H. and Christie, D. G., Transaction Society Glass Technology, Vol. 36T, 1952, p. 88.

31. Curran, D. R., Shockey, D. A., and Seaman, L., "Dynamic Fracture Criteria for a Polycarbonate," Journal Applied Physics, Vol. 44, 1973, pp. 4025-4038.

32. Schardin, H. and Struth, W., Z. tech. Phys., Vol. 18, 1937, p. 474.

33. Schardin, H. and Struth, W., Glastech. Ber., Vol. 16, 1938, p. 219.

34. Schardin, H., "Fracture Processes in Glass," Proceedings of the International Commission on Glass, Vol. I, 1954, pp. 81-95.

35. Schardin, H., "Velocity Effects in Fracture," Fracture, edited by B. L. Averbach, D. K. Felbeck, G. T. Hahn, and D. A. Thomas, New York: John Wiley and Sons, 1969.

36. Cotterell, B., "Velocity Effects in Fracture Propagation," Applied Material Research, 1965, pp. 327-332.

REFERENCES (Cont'd)

37. Dulaney, E. N. and Brace, W. F., "Velocity Behavior of a Growing Crack," Journal of Applied Physics, Vol. 31, 1960, pp. 2233-2236.

38. Roberts, D. K. and Wells, A. A., "The Velocity of Brittle Fracture," Engineering, December 24, 1954, pp. 820-821.

39. Wells, A. A. and Post, D., "The Dynamic Stress Distribution Surrounding a Running Crack - A Photoelastic Analysis," Proceedings SESA, Vol. 16, 1958, pp. 69-92.

40. Beebe, W. M., "An Experimental Investigation of Dynamic Crack Propagation in Plastics and Metals," AFML-TR-66-249, November 1966.

41. Kerkhof, F., "Ultrasonic Fractography," Proceedings of the Third International Congress on High Speed Photography, edited by R. B. Collins, London: Butterworth Scientific Publications, 1957, pp. 194-200.

42. Küppers, H., "The Initial Course of Crack Velocity in Glass Plates," International Journal of Fracture, Vol. 3, 1967, pp. 13-17.

43. Meagher, T. F. V. and Williams, D. C., "The Theory and Capabilities of Magnetically Driven Flyers," Kaman Nuclear, DASA-2440, June 1970.

44. Beebe, W. M., Jessey, M. E., Liu, H. W., Valluri, S. R., and Williams, M. L., "Development and Application of a High Speed Camera for Metallographic and Crack Propagation Studies," U.S. Air Force, Office of Aerospace Research ALR 64-69, April 1964.

45. Clark, A. B. J. and Sanford, R. J., "A Comparison of Static and Dynamic Properties of Photoelastic Materials," Proceedings SESA, Vol. 20(1), 1963, pp. 148-151.

46. Miklowitz, J., "The Propagation of Compression Waves in a Dispersive Elastic Rod - Part I - Results from the Theory," Journal of Applied Mechanics, Vol. 24, 1957, pp. 231-239.

47. Miklowitz, J. and Nisewanger, C. R., The Propagation of Compression Waves in a Dispersive Elastic Rod - Part II Experimental Results and Comparison with Theory," Journal of Applied Mechanics, Vol. 24, 1957, pp. 240-244.

REFERENCES (Cont'd)

48. Kolsky, H., Stress Waves in Solids, New York: Dover, 1963, p. 83.

49. Scott, R. A. and Miklowitz, J., "Transient Elastic Waves in Anisotropic Plates," Journal Applied Mechanics, Vol. 89E, 1967, pp. 104-110.

50. Glasoe, G. N. and Lebacqz, J. V., editors, Pulse Generators, New York: Dover, 1943.

51. Vlases, G. C., "Experiments in a Cylindrical Magnetic Shock Tube," Ph.D. Thesis, California Institute of Technology, Pasadena, California, 1963.

52. Chern, D. C. and Korneff, T., "Current Distribution for Wire Exploded in Vacuo," Exploding Wires, Vol. 4, Edited by W. G. Chace and H. K. Moore, New York: Plenum Press, 1968, pp. 173-183.

53. Dalley, J. W. and Riley, W. F., Experimental Stress Analysis, New York: McGraw-Hill, 1965.

54. Snell, R. F., MacKallor, D. C. and Guernsey, R., "An Electromagnetic Plane Stress-Wave Generator," MDAC Paper WD 1766, October 1971.

55. Döll, W., "Untersuchangen zam Bruchvorgang von verschieden molarem Polymethymethacrylat," Institut für Festkörpermechanik, Freiburg, West Germany, August 1974, p. 61.

56. Anderson, O. L., "The Griffith Criterion for Glass Fracture," Fracture, edited by B. L. Averbach, D. K. Felbeck, G. T. Hahn, and D. A. Thomas, New York: John Wiley and Sons, 1969, pp. 331-353.

57. Pucik, T. A., "Elastostatic Interaction of Cracks in the Infinite Plane," Ph.D. Thesis, California Institute of Technology, Pasadena, California, 1972.

58. Miklowitz, J., "Plane-Stress Unloading Waves Emanating from a Suddenly Punched Hole in a Stretched Plate," Journal of Applied Mechanics, Vol. 27, 1960, pp. 165-171.

59. Tada, H., Paris, P. and Irwin, G., The Stress Analysis of Cracks Handbook, Hellertown, Pennsylvania: Del Research Corporation, 1973, p. 3.6.

REFERENCES (Cont'd)

60. Dalley, J. W., Fourney, W. L., and Halloway, D. C., "A Dynamic Photoelastic Investigation of Explosive Induced Fracture," University of Maryland, August 1973.

61. Knauss, W. G., "Uniaxial Wave Propagation in a Viscoelastic Material Using Measured Material Properties," Journal of Applied Mechanics, Vol. 35, 1968, pp. 449-453.

62. Lee, E. H. and Kanter, I., "Wave Propagation in Finite Rods of Viscoelastic Materials," Journal of Applied Physics, Vol. 24, 1953, pp. 1115-1122.

63. Glauz, R. D. and Lee, E. H., "Transient Wave Analysis in a Linear Time Dependent Material," Journal of Applied Physics, Vol. 25, 1954, pp. 947-953.

64. Morrison, J. A., "Wave Propagation in Rods of Voigt Materials and Viscoelastic Materials with Three Parameter Models," Quarterly of Applied Mathematics, Vol. 14, 1956, pp. 153-169.

65. Arenz, R. J., "Uniaxial Wave Propagation in Realistic Viscoelastic Materials," Journal of Applied Mechanics, Vol. 31, No. 1, Trans. ASME, Vol. 86, Series E, March 1964, pp. 17-21.

66. Field, F. A., "A Simple Crack-Extension Criterion for Time-Dependent Spallation," Journal of the Mechanics and Physics of Solids, Vol. 19, 1971, pp. 61-70.

67. Dugdale, D. S., "Yielding of Steel Sheets Containing Slits," Journal of the Mechanics and Physics of Solids, Vol. 8, 1960, pp. 100-104.

68. Barenblatt, G. I., "The Mathematical Theory of Equilibrium Cracks in Brittle Fracture," Advances in Solid Mechanics, Vol. 7, 1962, pp. 56-131.

69. Weichert, R. and Schönert, K., "On the Temperature Rise at the Tip of a Fast Running Crack," Journal of the Mechanics and Physics of Solids, Vol. 22, 1974, pp. 127-133.

70. Rice, J. R., "Mathematical Analysis in the Mechanics of Fracture," Fracture, An Advanced Treatise, edited by H. Liebowitz, Academic Press, New York, 1968, pp. 192-314.

71. Goodier, J. N., and Field, F. A., "Plastic Energy Dissipation in Crack Propagation," Fracture of Solids, edited by D. C. Drucker and J. J. Gilman, Interscience Publishers, New York, 1963, pp. 103-118.

REFERENCES (Cont'd)

72. Fox, P. G., Fuller, K. N. G., "Thermal Mechanism for Craze Formation in Brittle Amorphous Polymers," Nature, Physical Science, Vol. 234, 1971, pp. 13-14.

73. Fuller, K. N. G., Fox, P. G., and Field, J. E., "The Temperature Rise at the Tip of Fast-Moving Cracks in Glassy Polymers," Proceedings of the Royal Society of London, Vol. 341, 1975, pp. 537-557.